Published for SISSA by Springer

Received: March 15, 2022
Revised: September 30, 2022
Accepted: November 14, 2022
Published: November 23, 2022

The flavourful present and future of 2HDMs at the collider energy frontier

Oliver Atkinson,[a] **Matthew Black,**[b] **Christoph Englert,**[a] **Alexander Lenz,**[b] **Aleksey Rusov**[b] **and James Wynne**[c]

[a] *SUPA, School of Physics & Astronomy, University of Glasgow, Glasgow G12 8QQ, U.K.*
[b] *Physik Department, Universität Siegen, Walter-Flex-Str. 3, 57068 Siegen, Germany*
[c] *IPPP, Department of Physics, University of Durham, DH1 3LE, U.K.*

E-mail: o.atkinson.1@research.gla.ac.uk, Matthew.Black@uni-siegen.de, christoph.englert@glasgow.ac.uk, Alexander.Lenz@uni-siegen.de, rusov@physik.uni-siegen.de, jameswynne39@gmail.com

Abstract: We study the intersection of flavour and collider physics for Two-Higgs-Doublet models of Type I and II. Drawing from the flavour precision-LHC exotics search complementarity, we also provide a projection of the future sensitivity that can be achieved in light of currently available analyses. On the one hand, we find that the parameter space of the 2HDM can be explored significantly further with more data from the LHC with some complementarity with flavour physics. On the other hand, flavour physics results alongside their projections remain powerful tools to constrain the model space in regions where direct sensitivity to new states via exotics searches is lost. Our results further highlight the recently observed flavour physics anomalies as important drivers of new physics searches in the future; we also touch on implications for a strong first order electroweak phase transition.

Keywords: Multi-Higgs Models, Higgs Properties

ArXiv ePrint: 2202.08807

https://doi.org/10.1007/JHEP11(2022)139

JHEP11(2022)139

Contents

JHEP11(2022)139

1 Introduction

Searches for physics beyond the Standard Model (BSM) are key pillars of the current particle physics programme that stretches across many different experimental arenas. Shortcomings of the Standard Model (SM), e.g. the possible lack of enough CP violation or the insufficiently strong electroweak phase transition to address the Sakharov criteria [1], provide the motivation for extending the interaction and particle spectrum of the SM. Especially well-motivated scenarios along these lines are Higgs sector extensions. While the existence of a non-trivial electroweak vacuum structure had been verified with the discovery of the W and Z bosons at UA1/UA2, it was only in 2012 that the discovery of the Higgs boson [2, 3] confirmed the mechanism of spontaneous symmetry breaking [4–6] through the Higgs boson's couplings to the massive gauge bosons. Subsequent investigations of the 125 GeV Higgs boson after its discovery have shown that this new state closely follows the SM expectation. Nonetheless, current experimental constraints only limit modification of

the Higgs boson's interactions to be below $\sim 10\%$ [7, 8] so there are reasonable margins for new, weakly-coupled modifications of the Higgs sector. Consistency with electroweak fits [9] provides an additional constraint for extensions of the symmetry breaking Higgs sector that can be competitive with current direct measurements.

Out of the Higgs sector extensions that are typically considered for BSM investigations, two Higgs doublet models (2HDMs) are particularly well-motivated theories (for reviews see refs. [10, 11]). On the one hand, they implement custodial isospin analogous to the SM Higgs field, thus avoiding tensions and fine-tuning with electroweak precision measurements that occur in higher dimensional representations of electroweak $SU(2)_L \times U(1)_Y$ breaking [12]. On the other hand, 2HDMs can be considered as harbingers of supersymmetric theories, which demand a second Higgs doublet due to holomorphy, and (non-)perturbative anomaly cancellation to maximise the S-matrix symmetry.

Leaving aside the theoretical motivation for introducing a second weak doublet contributing to electroweak symmetry breaking and fermion mass generation, the experimental avenues to constrain or even observe a 2HDM extension of the SM are plentiful: links of fermion vs. gauge boson mass generation provide a motivation to combine precision flavour physics investigations with those performed at the high energy frontier, chiefly at the Large Hadron Collider (LHC). In fact, a recent investigation into the flavour and Higgs signal strength constraints of the 2HDM [13] demonstrated the power of flavour measurements in driving BSM mass scales into a region where the direct detection at the LHC could become challenging. Additionally, current flavour anomalies highlight flavour physics as a particularly relevant area to inform future investigations at the high energy frontier.

Building on ref. [13], we investigate the intersection of flavour and collider physics for the 2HDMs of type I and II in this work, with a view towards the High Luminosity (HL) LHC phase. Clarifying and extrapolating the currently available search strategies in flavour physics and for the exotic states that are predicted in the 2HDM enables us to discuss flavour-collider complementarity and identify regions that require targeting to enhance the BSM potential during the upcoming LHC runs.

We organise this work as follows: in section 2, we review the basics of the 2HDM to make this work self-consistent. Section 3 provides details on theoretical and electroweak constraints that set the baseline of our investigation, then in section 4 we discuss the status of the SM Higgs signal strengths in the 2HDM type I (2HDM-I). In section 5 we discuss in detail the flavour constraints on the 2HDM-I, extending the work of ref. [13], before we move on to contrast LHC searches and measurements in section 6 for the 2HDM-I and 2HDM-II. We also comment on expected improvements of both flavour and collider constraints before discussing cosmological implications in section 7. We provide a summary and conclusions in section 8.

2 The two Higgs doublet model

We follow the notation of refs. [10, 11], where, instead of using the SM Higgs doublet and its (symplectic) charge-conjugated version to gain mass terms for both up-type and

JHEP11(2022)139

Model	I	II	X	Y
u_R^i	Φ_2	Φ_2	Φ_2	Φ_2
d_R^i	Φ_2	Φ_1	Φ_2	Φ_1
e_R^i	Φ_2	Φ_1	Φ_1	Φ_2

Table 1. Types of 2HDM with natural flavour conservation from demanding fermions couple to specific doublets.

down-type quarks, one can introduce two distinct doublets

$$\Phi_i = \begin{pmatrix} \phi_i^+ \\ (v_i + \phi_i^0 + iG_i^0)/\sqrt{2} \end{pmatrix}, \tag{2.1}$$

with $i = 1, 2$. After electroweak symmetry breaking (EWSB), these doublets lead to 5 physical Higgs bosons (the other 3 degrees of freedom construct the longitudinal $W^\pm$, Z^0 boson polarisations). One finds two charged Higgs, $H^\pm$, two neutral scalars, h^0, H^0, and a neutral pseudoscalar, A^0. We take h^0 to be the lighter of the two neutral scalars and the currently observed Higgs particle with mass $125.25 \pm 0.17\,\text{GeV}$ [14]. The potential for a general 2HDM with a softly broken $\mathbb{Z}_2$ symmetry is [10]

$$\begin{aligned} V(\Phi_1, \Phi_2) = {} & m_{11}^2 \Phi_1^\dagger \Phi_1 + m_{22}^2 \Phi_2^\dagger \Phi_2 - m_{12}^2 (\Phi_1^\dagger \Phi_2 + \Phi_2^\dagger \Phi_1) + \frac{\lambda_1}{2} (\Phi_1^\dagger \Phi_1)^2 + \frac{\lambda_2}{2} (\Phi_2^\dagger \Phi_2)^2 \\ & + \lambda_3 (\Phi_1^\dagger \Phi_1)(\Phi_2^\dagger \Phi_2) + \lambda_4 (\Phi_1^\dagger \Phi_2)(\Phi_2^\dagger \Phi_1) + \frac{\lambda_5}{2} \left[(\Phi_1^\dagger \Phi_2)^2 + (\Phi_2^\dagger \Phi_1)^2 \right]. \end{aligned} \tag{2.2}$$

We can use this potential in its "lambda basis" to construct mass terms for each of the physical Higgs particles, which, alongside the vacuum expectation value (VEV) $v^2 = v_1^2 + v_2^2$, the ratio of VEVs $\tan\beta = v_2/v_1$, the mixing parameter $\cos(\beta - \alpha)$, and the softly $\mathbb{Z}_2$ breaking term m_{12} form the "mass basis" which more simply translates to physical observables, see e.g. refs. [13, 15–18] for transformations between bases.

The Yukawa couplings in the 2HDM can be generally expressed as

$$\mathcal{L}_Y = -y_{ij}^1 \bar{\Psi}_L^i \Phi_1 \psi_R^j - y_{ij}^2 \bar{\Psi}_L^i \Phi_2 \psi_R^j . \tag{2.3}$$

In general the 2HDM Yukawa couplings need not be flavour diagonal and so it is possible to allow tree-level flavour-changing neutral currents (FCNCs) which are absent in the SM. In order to maintain this natural flavour conservation, one can consider fermions coupling to the Higgs doublets in specific ways. The four types of 2HDM with natural flavour conservation are described in table 1. After spontaneous symmetry breaking, we can write the Yukawa sector of the 2HDM Lagrangian as (see e.g. refs. [10, 19])

$$\begin{aligned} \mathcal{L}_{\text{Yukawa}}^{\text{2HDM}} = {} & - \sum_{f=u,d,\ell} \frac{m_f}{v} \left(\xi_h^f \, \bar{f} f h + \xi_H^f \, \bar{f} f H + i \eta_f \xi_A^f \, \bar{f} \gamma_5 f A \right) \\ & - \left[\frac{\sqrt{2} V_{ud}}{v} \bar{u} \left(m_d \, \xi_A^d P_R - m_u \, \xi_A^u P_L \right) d H^+ + \frac{\sqrt{2}}{v} m_\ell \, \xi_A^l (\bar{\nu} P_R \ell) H^+ + \text{h.c.} \right], \end{aligned} \tag{2.4}$$

JHEP11(2022)139

Model	I	II	X	Y
ξ_h^u	$\cos\alpha/\sin\beta$	$\cos\alpha/\sin\beta$	$\cos\alpha/\sin\beta$	$\cos\alpha/\sin\beta$
ξ_h^d	$\cos\alpha/\sin\beta$	$-\sin\alpha/\cos\beta$	$\cos\alpha/\sin\beta$	$-\sin\alpha/\cos\beta$
ξ_h^l	$\cos\alpha/\sin\beta$	$-\sin\alpha/\cos\beta$	$-\sin\alpha/\cos\beta$	$\cos\alpha/\sin\beta$
ξ_H^u	$\sin\alpha/\sin\beta$	$\sin\alpha/\sin\beta$	$\sin\alpha/\sin\beta$	$\sin\alpha/\sin\beta$
ξ_H^d	$\sin\alpha/\sin\beta$	$\cos\alpha/\cos\beta$	$\sin\alpha/\sin\beta$	$\cos\alpha/\cos\beta$
ξ_H^l	$\sin\alpha/\sin\beta$	$\cos\alpha/\cos\beta$	$\cos\alpha/\cos\beta$	$\sin\alpha/\sin\beta$
ξ_A^u	$\cot\beta$	$\cot\beta$	$\cot\beta$	$\cot\beta$
ξ_A^d	$\cot\beta$	$-\tan\beta$	$\cot\beta$	$-\tan\beta$
ξ_A^l	$\cot\beta$	$-\tan\beta$	$-\tan\beta$	$\cot\beta$

Table 2. Coupling strengths ξ in each type of 2HDM between the Higgs particles and fermions.

where the factor η_f for fermion type $f = d, \ell$ is 1 and for $f = u$ is -1. Imposing the fermion interactions to specific doublets in table 1, the ξ coupling strengths are expressed in table 2.[1]

3 Theory and electroweak precision constraints

3.1 Perturbativity, unitarity, and vacuum stability

Perturbativity in the scalar sector can be simply expressed as [20, 21]

$$|\lambda_i| \leq 4\pi, \qquad i = 1, \ldots 5. \tag{3.1}$$

As in ref. [13] we also consider the less conservative bounds of $|\lambda_i| \leq 4$ — inspired by the results in refs. [22, 23]. Looking at the couplings in eq. (2.4), one can further consider the perturbativity constraints from the Yukawa sector:

$$\frac{\sqrt{2}\, V_{tb}\, m_t \cot\beta}{2v} \leq \sqrt{4\pi} \quad \Longrightarrow \quad \tan\beta > 0.14\,, \tag{3.2}$$

where we have chosen a very conservative range. For the range of $\log[\tan\beta]$ we will consider the conservative lower bound $\tan\beta = 10^{-1.5} \approx 0.03$, in line with the above perturbativity result. In the 2HDM-I there is no corresponding upper bound from perturbativity considerations as the Higgs couplings to fermions are each proportional to $\cot\beta$, however here we adopt $\tan\beta = 10^{+2.5} \approx 300$ as an upper limit and note that extending to higher $\tan\beta$ would not significantly change our results due to the couplings being minimal at large $\tan\beta$. This is the same limit adopted in ref. [13], which is motivated by perturbativity considerations from the charged Higgs coupling to the b quark, thereby allowing for straightforward comparison of results between 2HDM-II [13] and 2HDM-I (this work).

We apply the conditions for a stable vacuum as set out in ref. [24], whilst demanding the vacuum to be the global minimum of the potential [25]. We also consider the conditions from tree-level unitarity, see refs. [21, 26],[2] alongside NLO unitarity and the condition that

[1] Note that we differ from ref. [10] by a sign in the H^+ Yukawa interaction which in turn leads to a difference in the fermion coupling strengths. This is the same convention as found in e.g. ref. [19].

[2] For a similar discussion in an alternative lambda basis see ref. [27].

JHEP11(2022)139

NLO corrections to partial wave amplitudes are suppressed relative to LO contributions, see refs. [22, 23].

We get the same constraints on the 2HDM parameters as found in our previous study from theory, where these are not dependent on the specific couplings defining the different types of 2HDM. We refer to figure 1 of ref. [13] for these results, where the main implication is a close mass degeneracy for the new Higgses enforced from $\sim 1\,\text{TeV}$ and becomes stricter as the mass scale increases.

3.2 Oblique corrections

The expressions for the electroweak precision observables (EWPOs): S, T, and U [28, 29] (also referred to as oblique corrections) in the 2HDM (derived from ref. [30]) are explicitly given in appendix C of ref. [13]. New physics generally has only a small effect on U in comparison to the S and T parameters as the latter correspond to distinct dimension 6 operators in the effective field theory expansion, in contrast to U [31]. It is therefore justified to follow the approach that neglects U from fits by setting $U = 0$ as outlined in refs. [9, 14]. This effectively reduces the error on the experimental result for T, due to the correlation between T and U. The oblique parameters will be included in our global fit.

4 Higgs signal strengths

Many measurements of the properties of the observed Higgs boson have been made. Of these, the most relevant for our discussion are the Higgs signal strengths μ_i^f, which are defined as a ratio between experimental and SM values of the product of the cross section and branching fraction in a given channel with production mode i and decay products f:

$$\mu_i^f = \frac{(\sigma_i \cdot \mathcal{B}_f)_{\text{Exp.}}}{(\sigma_i \cdot \mathcal{B}_f)_{\text{SM}}}. \tag{4.1}$$

Measurements of μ_i^f essentially serve as an indicator of how closely the observed Higgs matches the SM expectations. We include results from 31 channels [8, 32–37] (collected in table 4 of ref. [13]).

If the observed Higgs is not that of the SM, but part of an extended Higgs sector such as the 2HDM, its couplings to other particles will differ from the SM, a difference that will feed through into the values of the signal strengths. This is the case in the 2HDM-I, with the couplings being modified by the factors shown in table 2. It is therefore possible to use the signal strength measurements to constrain the parameters on which these couplings depend, namely the mixing angles. We do this by performing a fit using analytical calculations of the signal strengths in the 2HDM-I as functions of the input parameters $\tan\beta$ and $\cos(\beta-\alpha)$ from expressions given in ref. [11], with results presented in figure 1. Opposed to the 2HDM-II case (see ref. [13]) we find that more sizeable deviations from the alignment limit $\cos(\beta-\alpha) = 0$ are allowed for the 2HDM-I. We observe that larger deviations from the alignment limit are possible with increasing $\tan\beta$, and we find $|\cos(\beta-\alpha)| \leq 0.21\ (0.4)$ at $2\ (5)\sigma$ for sufficiently large $\tan\beta \geq 10$.

JHEP11(2022)139

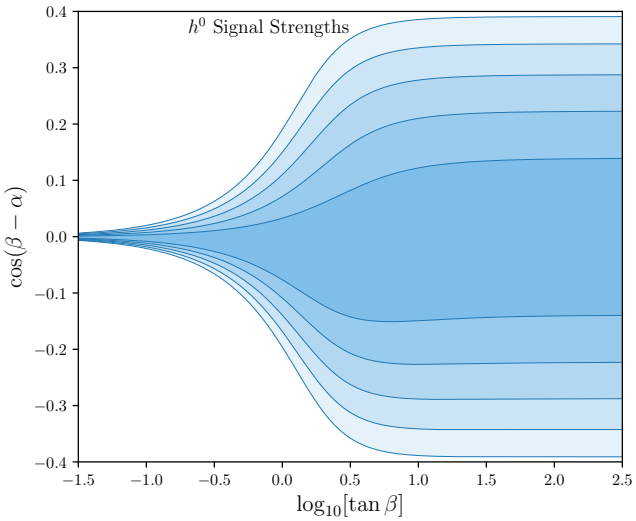

Figure 1. Combined fits of the SM Higgs signal strengths in the 2HDM-I (in the $(\tan\beta - \cos(\beta-\alpha))$ plane). Contours are shown representing allowed parameter space at 1, 2, 3, 4, 5σ confidence from darkest to lightest.

5 Flavour constraints in 2HDM-I

In section 5.1, we cover the constraints on the 2HDM-I parameter space from flavour observables, and then in section 5.2 we combine these with the Higgs signal strengths and the EWPOs. We follow the procedure of the earlier study [13] in the 2HDM-II, where we now exchange the Type II couplings for the Type I. All observables we consider here are listed with SM predictions and experimental measurements in tables 4-8 of ref. [13]; the measurements are collected from various results throughout literature [8, 14, 32, 33, 35–66] and the SM predictions are calculated in **flavio** unless otherwise stated.

5.1 Individual fits

For the tree-level (semi-)leptonic flavour-changing charged transitions, the 2HDM-I contributes through the effective operators

$$\mathcal{O}_{S-P} = (\bar{u}P_L\, d)(\bar{\ell}P_L\nu_\ell), \qquad \mathcal{O}_{S+P} = (\bar{u}P_R\, d)(\bar{\ell}P_L\nu_\ell), \tag{5.1}$$

with $P_{L(R)} = (1 \mp \gamma_5)/2$. The Wilson coefficients of these operators in terms of the 2HDM-I parameters are

$$C_{S-P} = -\frac{m_u\, m_\ell \cot^2\beta}{m_{H^+}^2}, \qquad C_{S+P} = \frac{m_d\, m_\ell \cot^2\beta}{m_{H^+}^2}\,. \tag{5.2}$$

For a description of all operators gaining contributions from the 2HDM for the observables we consider and the translation of basis for these, we refer to [13], taking expressions for the Wilson coefficients from refs. [19, 67–69] where these are expressed in terms of general 2HDMs and one can simply insert the appropriate couplings for the 2HDM-I.

First we consider the Lepton-Flavour Universality (LFU) observables $R(D^{(*)}) \equiv \mathcal{B}(B \to D^{(*)}\tau\bar{\nu}_\tau)/\mathcal{B}(B \to D^{(*)}\ell\bar{\nu}_\ell)$, where $\ell = e, \mu$. The latter implies a 2.8σ tension

JHEP11(2022)139

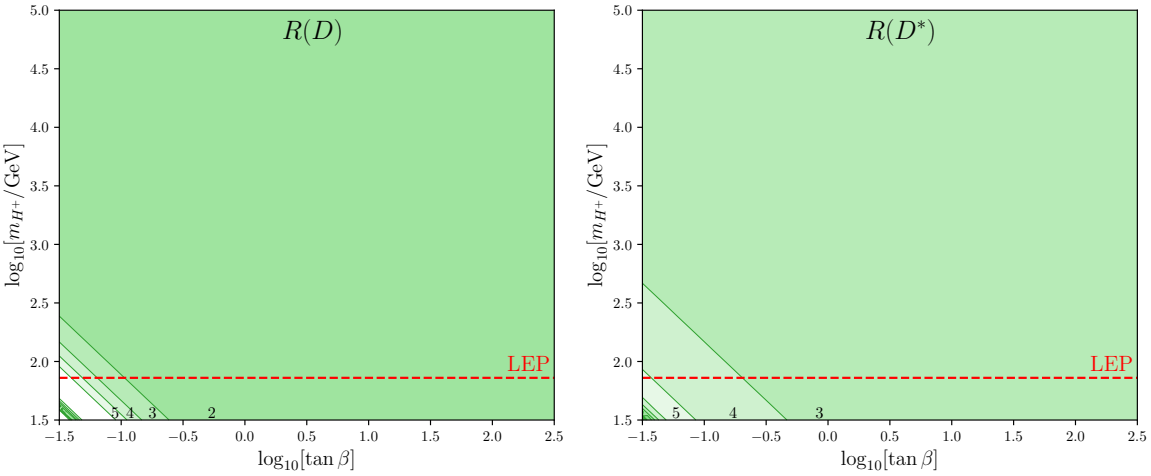

Figure 2. Contour plots of the allowed 2HDM-I parameter space in the $(\tan\beta - m_{H^+})$ plane for $R(D)$ (left) and $R(D^*)$ (right). Contours are shown representing allowed parameter space at 1, 2, 3, 4, 5σ confidence from darkest to lightest; the confidence in σ is also written inside each contour region for clarity (outside the tiny regions in the very lower left of the plots). The red dashed line indicates the LEP lower bound for m_{H^+} in the Type I 2HDM (72.5 GeV).

between experimental measurements and SM predictions, and the combined tension of the two between experiment and the SM is 3.2σ (using **flavio**). We show in figure 2 the allowed 2HDM-I parameter space for these two observables in individual fits. Within the theoretically-motivated parameter limits of our fits, we find that $R(D)$ allows a large part of our parameter space within 2σ, whereas $R(D^*)$ allows most of our parameter space at 2.8σ or above. In fact, for both observables, we find the best fit for $m_{H^+} \sim 1\,\text{GeV}$ which is outside the physical domain of our model. Within the considered limits of our parameters, we find a minimum of 3.5σ combined tension between the 2HDM-I and experiment for $R(D^{(*)})$. In figure 3, we present the combined fit of tree-level flavour-changing charged currents including leptonic and semi-leptonic decays of mesons, hadronic decays of τ leptons, and $R(D^{(*)})$; see table 6 of ref. [13] for all channels considered. The SM predictions in **flavio** for the leptonic and semi-leptonic channels are based on refs. [70–78], and the new 2HDM-I contributions are described by eq. (5.2).

Next we consider the mixing of neutral $B_{d,s}$ mesons. The mass differences of this meson mixing are experimentally known very precisely at the level $\sim \mathcal{O}(0.1\%)$ [14]. On the theory side, however, the uncertainties are still dominated by the non-perturbative determinations of the matrix elements of the $\Delta B = 2$ operators. We use the averages presented in ref. [79] combining HQET Sum Rules [80–82] and lattice calculations [83–85], yielding a theory precision of $\mathcal{O}(5\%)$. Terms proportional to the tH^- coupling dominate the 2HDM contributions in the box diagrams with the down-type quark effects largely mass-suppressed. The predictions in the 2HDM-I for B-meson mixing are therefore very similar to those in the 2HDM-II where the dominating up-type $H^\pm$ couplings remain the same. The combined fit for $\Delta m_{d,s}$ is shown in figure 4, where we find a correlation between $\tan\beta$ and m_{H^+} constraining $\tan\beta$ from below. We take the expressions for the $\Delta B = 2$ Wilson coefficients from ref. [19], converting to the **flavio** basis as described in ref. [13].

JHEP11(2022)139

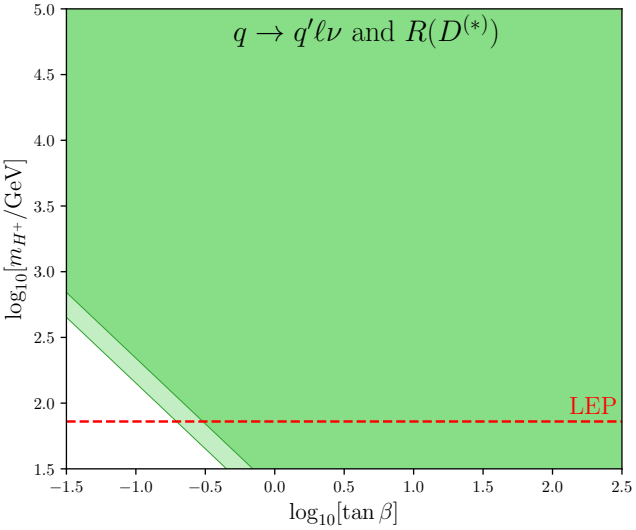

Figure 3. Contour plot of the allowed 2HDM-I parameter space in the $(\tan\beta - m_{H^+})$ plane for the combination of tree-level leptonic and semi-leptonic decays of B, B_s, D, D_s, K, and π mesons and the hadronic decays of τ leptons to K and π mesons with a tau neutrino as well as $R(D)$ and $R(D^*)$. The lighter contour indicates the allowed parameter space at 2σ confidence level while the darker contour corresponds to 1σ. The red dashed line indicates the LEP lower bound for m_{H^+} in the Type I 2HDM (72.5 GeV).

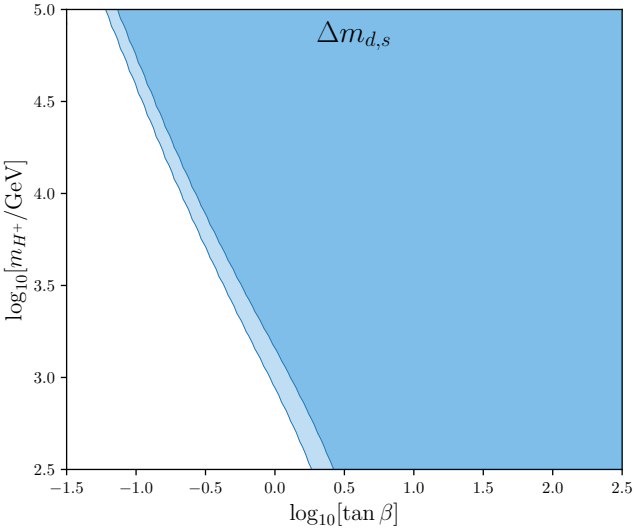

Figure 4. Contour plot of the allowed 2HDM-I parameter space in the $(\tan\beta - m_{H^+})$ plane for the combined fit to $\Delta m_{d,s}$. The darker contour indicates allowed parameter space at 1σ confidence, and the lighter at 2σ.

JHEP11(2022)139

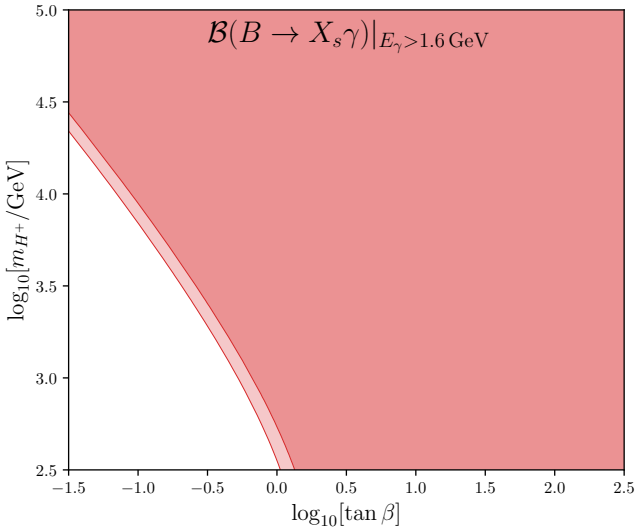

Figure 5. Contour plot of the allowed 2HDM-I parameter space in the $(\tan\beta - m_{H^+})$ plane for $\mathcal{B}(\bar{B} \to X_s\gamma)$. The darker contour indicates allowed parameter space at 1σ confidence, and the lighter at 2σ.

A signature observable for new physics analysis is the branching ratio of the $\bar{B} \to X_s\gamma$ decay. In the SM, this is known to NNLO in QCD [86] (based on the previous refs. [87, 88]). We take the experimental average [43] formed from refs. [89–91]. In the 2HDM-II, $\bar{B} \to X_s\gamma$ provides a distinct constraint on the lower bound for the charged Higgs mass m_{H^+}; in the Type I however, this is much more correlated with $\tan\beta$, and we therefore cannot find a clear constraint from this observable alone. In figure 5 we show the fit to $\mathcal{B}(\bar{B} \to X_s\gamma)|_{E_\gamma > 1.6\,\mathrm{GeV}}$ in the 2HDM-I where we calculate the contributions to the Wilson coefficients C_7, C_8 at NLO using refs. [68, 69].

We also consider the FCNC processes $B_{d,s} \to \mu^+\mu^-$, which are sensitive to BSM contributions to scalar operators, making them important observables to test the 2HDM. In recent years, ATLAS, CMS, and LHCb [92–97] have all produced measurements for $B_s \to \mu^+\mu^-$, and developed further the upper limit on $B_d \to \mu^+\mu^-$. In our analysis we make use of the combination of these measurements from ref. [47]. The theory prediction is formed of the perturbative calculations [98–100] and the determinations of the non-perturbative decay constants, for example [101–103]. The 2HDM Wilson coefficients (taken again from ref. [19]) for the operators contributing to these processes, $\mathcal{O}_{10}^{(\prime)}, \mathcal{O}_S^{(\prime)}, \mathcal{O}_P^{(\prime)}$, also depend on further 2HDM parameters: $\cos(\beta - \alpha), m_{H^0}, m_{A^0}$. Motivated by constraints from theory and the Higgs signal strengths (see sections 3 and 4), we present in figure 6 a 2D fit in the $(\tan\beta - m_{H^+})$-plane fixing $\cos(\beta - \alpha) = 0$ and $m_{H^0} = m_{A^0} = m_{H^+}$. In this approach, we find here similarly to $\bar{B} \to X_s\gamma$ a strong correlation between $\tan\beta$ and m_{H^+}. Later in our global fit (section 5.2), we will discuss further the dependence on these additional parameters.

The LFU ratios R_K and R_{K^*} [104] have become well-studied processes in recent years (see e.g. refs. [105–112]), driven by LHCb measurements [64, 65] finding discrepancies with the SM, most noticeably the deviation of 3.1σ in R_{K^+} [63]. Model-independent analyses (for

JHEP11(2022)139

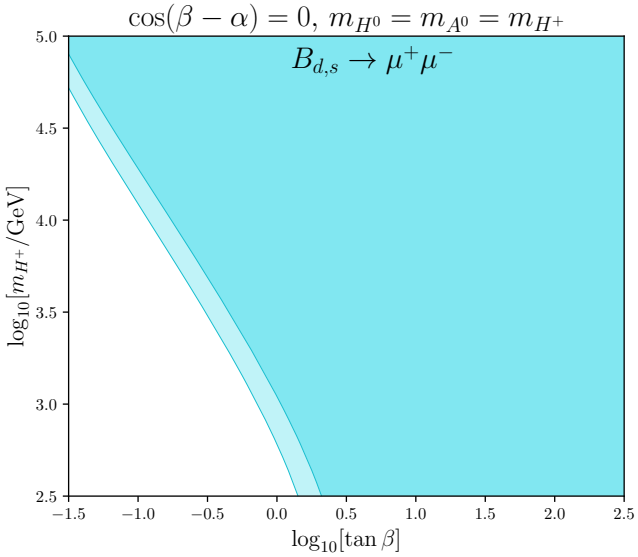

Figure 6. Contour plot of the allowed 2HDM-I parameter space in the $(\tan\beta - m_{H^+})$ plane for the combined fit to $(B_{d,s} \to \mu^+\mu^-)$, taken in the limits of alignment $(\cos(\beta-\alpha)=0)$ and degenerate masses $(m_{H^0} = m_{A^0} = m_{H^+})$. The darker contour indicates allowed parameter space at 1σ confidence, and the lighter at 2σ.

example, refs. [113–117]) show these processes favour vector-like new physics contributing to $\mathcal{O}_{9,10}$ for their deviations to be resolved. In the large $\tan\beta$ limit we recover the SM predictions, as the 2HDM-I induced coupling deviations will go to zero. With the SM result equating to our best fit point, no point in our parameter space can reduce the tensions in these observables beyond their current status. In figure 7, we show our combined fit for the 10 $R_{K^{(*)}}$ bins within a more similar parameter region to other fits, where we see that most of our parameter space considered lies within 1σ of the SM result. Within 1σ we find two regions disconnected from each other in figure 7; in principle, one should only expect the right-most region at 1σ, however there can exist a "fine-tuned" solution for observables in the 2HDM where the configuration of m_{H^+} and $\tan\beta$ is such that the 2HDM contribution cancels outside of the decoupling limit and we approach the SM result again. The left 1σ region in figure 7 results from the combination of these "fine-tuned" solutions for both the K and K^* modes, where the different structures of these solutions between the modes and the tensions in different bins combine to stretch this region out into the shape we see.
A discovered 2HDM-I within the physical bounds of the model could only increase the tensions in $R_{K^{(*)}}$ as we find them currently in the SM.

In figure 8, we consider more $b \to s\ell^+\ell^-$ observables (see table 7 in ref. [13]), where some of these also find tension with experiment in the SM. For detailed descriptions and analyses focused specifically on this interesting group of observables, see e.g. refs. [47, 73, 106, 108, 111–114, 118–126]. Similarly to R_K and R_{K^*} above, these processes tend to favour new physics (NP) contributions from $\mathcal{O}^{(\prime)}_{9,10}$. In the 2HDM-I, we find that the contributions to these operators (and also to $\mathcal{O}^{(\prime)}_{S,P}$) can be sufficient to reduce the tension with experiment for a large group of the $b \to s\ell\ell$ observables including, among others,

JHEP11(2022)139

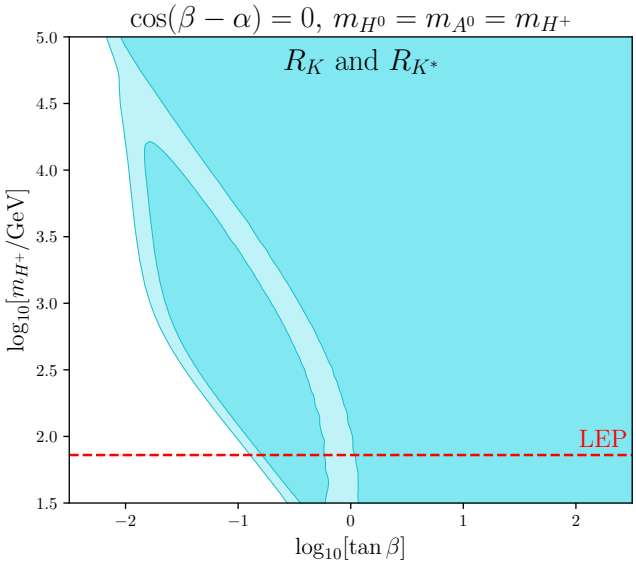

Figure 7. Contour plot of the allowed 2HDM-I parameter space in the $(\tan\beta - m_{H^+})$ plane for the combined fit to the 10 $R_{K^{(*)}}$ bins in table, taken in the limits of alignment $(\cos(\beta-\alpha)=0)$ and degenerate masses $(m_{H^0}=m_{A^0}=m_{H^+})$. The darker contour indicates allowed parameter space at 1σ confidence, and the lighter at 2σ. The red dashed line indicates the LEP lower bound for m_{H^+} in the Type I 2HDM (72.5 GeV).

binned angular observables in $B \to K^*\ell\ell$. This effect is most significant for $m_{H^0} \sim m_{A^0} \sim m_{H^+} \sim 1000\,\mathrm{GeV}$ as suggested by the best-fit point in table 3, where we find an improvement over the SM with a pull of 2.6σ (excluding $R_{K^{(*)}}$); we then find a large portion of our parameter space within 1σ confidence of this result. Varying all 2HDM parameters around the best fit point, we also find that this group of observables imposes a lower bound on $\tan\beta$ as

$$\tan\beta \gtrsim 0.14\,(0.16) \quad \text{at } 2\sigma\,(1\sigma), \tag{5.3}$$

which is compatible with the lower bound coming from perturbativity in section 3. This lower bound is numerically very similar to that seen from the one parameter configuration used in figure 8, implying that, within the limits used in our analysis, this lower bound depends only minimally on the additional parameters.

5.2 Global fits

We now consider our global fits to the 2HDM-I combining flavour observables, Higgs signal strengths, and the EWPOs S, T, U. Within the contours of a global fit, the LFU ratios $R_{D^{(*)}}$, $R_{K^{(*)}}$ still have a tension $\sim 3.5\sigma$ with experiment that is worsened compared to the SM.[3] This motivates two scenarios for the global fits: either including these LFU ratios, or considering a fit excluding them. In table 3, we summarise the results of the various fits performed, indicating their best-fit parameter points and the corresponding

[3]Some other $b \to s\ell\ell$ observables still find some tension, but these are not as severe and are lessened compared to the SM.

JHEP11(2022)139

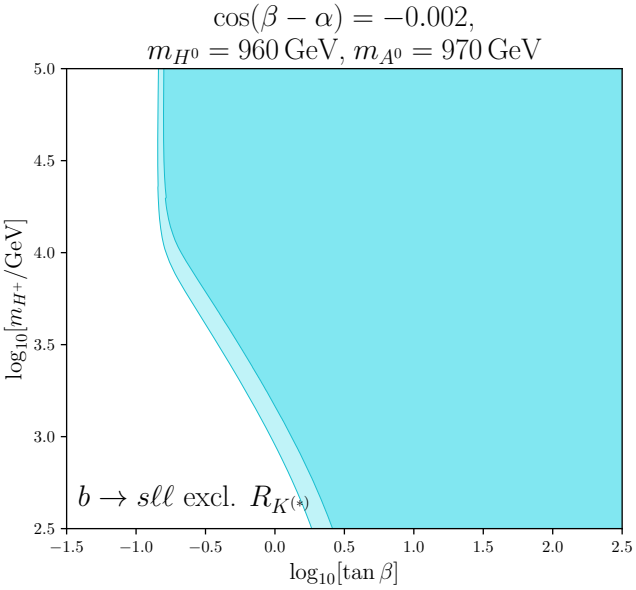

Figure 8. Contour plot of the allowed 2HDM-I parameter space in the $(\tan\beta - m_{H^+})$ plane for the combined fit to the leptonic $B_{d,s} \to \mu^+\mu^-$ decays and the semi-leptonic $b \to s\ell^+\ell^-$ observables, excluding $R_{K^{(*)}}$ and fixing the additional parameters to their best-fit points. The darker contour indicates allowed parameter space at 1σ confidence, and the lighter at 2σ.

statistics. In figure 9, we show the fit to all observables (excluding $R_{D^{(*)},K^{(*)}}$) where we fix the additional 2HDM parameters to their best fit point as shown in table 3. We include the left plot of figure 9 as an example of how these fits can change in different limits for the additional parameters, however it is important to note that due to the theoretical bounds on the masses in the 2HDM, this plot covers parameter space not wholly valid and by itself cannot inform our final parameter constraints. In figure 10, we show the fit to all observables (excluding $R_{D^{(*)},K^{(*)}}$) in the alignment limit and with degenerate masses. We find the shapes of the contours to be much the same for excluding/including $R_{D^{(*)},K^{(*)}}$, so we do not show both sets of plots here; the impact of including $R_{D^{(*)},K^{(*)}}$ is clearer in table 3, where we find distinctly poorer quality of fit (low p-value) in this scenario. Excluding $R_{D^{(*)},K^{(*)}}$, we find a pull of 1.9σ improvement from the SM to 2HDM-I; including $R_{D^{(*)},K^{(*)}}$, the improvement is 1.5σ.

From table 3, we see that $\cos(\beta - \alpha) = 0$ (the alignment limit) is closely favoured from the fits, although figure 9 shows that larger deviations from alignment are allowed than in the 2HDM-II. We find preference in the global fits for $\tan\beta \sim \mathcal{O}(100)$ and $m_{H^+} \sim m_{H^0} \sim m_{A^0} \sim 1.7\,\text{TeV}$, where a closer mass degeneracy at this scale is enforced from theory constraints. Within the parameter region found we scan around the best fit point to find the full constraints on our parameters. As one can see throughout this section, much of the small $\tan\beta$ parameter space is excluded by most observables individually and globally. We cannot state an explicit bound on $\tan\beta$ from the global fit however as the lower limit is clearly correlated with the charged Higgs mass. For the mass of the charged Higgs, within

JHEP11(2022)139

Scenario	# Observables	Best-fit point $\{\tan\beta, m_{H^+}, m_{H^0}, m_{A^0}, \cos(\beta-\alpha)\}$	χ^2_{min}	p-value
All incl. $R_{D^{(*)},K^{(*)}}$	275	$\{70, 1720\,\text{GeV}, 1680\,\text{GeV}, 1670\,\text{GeV}, -0.001\}$	317.0	2.6%
All excl. $R_{D^{(*)},K^{(*)}}$	263	$\{80, 1720\,\text{GeV}, 1770\,\text{GeV}, 1770\,\text{GeV}, -0.003\}$	281.1	15.5%
Flavour incl. $R_{D^{(*)},K^{(*)}}$	241	$\{60, 1650\,\text{GeV}, 1600\,\text{GeV}, 1600\,\text{GeV}, -0.002\}$	289.1	1.0%
Flavour excl. $R_{D^{(*)},K^{(*)}}$	229	$\{30, 1790\,\text{GeV}, 1750\,\text{GeV}, 1740\,\text{GeV}, -0.002\}$	249.4	11.7%
$b \to s\ell\ell$ incl. $R_{K^{(*)}}$	202	$\{40, 1030\,\text{GeV}, 920\,\text{GeV}, 1010\,\text{GeV}, -0.003\}$	262.1	0.1%
$b \to s\ell\ell$ excl. $R_{K^{(*)}}$	192	$\{35, 1020\,\text{GeV}, 960\,\text{GeV}, 970\,\text{GeV}, -0.002\}$	234.4	1.1%
Higgs Signals	31	$\{> 1000, --, --, --, 0.0\}$	28.2	50.7%
Alignment Limit, $\cos(\beta-\alpha)=0$				
All incl. $R_{D^{(*)},K^{(*)}}$	275	$\{40, 1760\,\text{GeV}, 1730\,\text{GeV}, 1690\,\text{GeV}\}$	318.5	2.5%
All excl. $R_{D^{(*)},K^{(*)}}$	263	$\{50, 1810\,\text{GeV}, 1750\,\text{GeV}, 1760\,\text{GeV}\}$	283.7	13.9%
$\cos(\beta-\alpha)=0$, $m_{H^+}=m_{H^0}=m_{A^0}$				
All incl. $R_{D^{(*)},K^{(*)}}$	275	$\{90, 1630\,\text{GeV}\}$	324.3	1.8%
All excl. $R_{D^{(*)},K^{(*)}}$	263	$\{80, 1750\,\text{GeV}\}$	286.4	13.9%

Table 3. Best fit points of 2HDM-I parameter fits for various groups of observables using the constraints from theory to inform the physical parameter values.

the parameter region we test, we find bounds only at 1σ confidence:

$$m_{H^+} \leq 83.4\,\text{TeV} \quad \text{at } 1\sigma. \tag{5.4}$$

In our global fit of all observables, our constraints on $\cos(\beta-\alpha)$ are much improved from considering the Higgs signal strengths alone, where we find the constraints in the full analysis to follow very closely to the representative plot in figure 9:

$$\begin{aligned} |\cos(\beta-\alpha)| &\leq 0.11 \quad \text{at } 1\sigma, \\ |\cos(\beta-\alpha)| &\leq 0.14 \quad \text{at } 2\sigma, \\ |\cos(\beta-\alpha)| &\leq 0.17 \quad \text{at } 3\sigma, \\ |\cos(\beta-\alpha)| &\leq 0.19 \quad \text{at } 4\sigma, \\ |\cos(\beta-\alpha)| &\leq 0.21 \quad \text{at } 5\sigma. \end{aligned} \tag{5.5}$$

5.3 Comment on the muon anomalous magnetic moment

It is worthwhile to comment on the anomalous magnetic moment of the muon, a_μ, which we do not include in our overall fit. The recent results from Run 1 at Fermilab [127] confirmed the previous result from BNL [128], where the combined experimental value now yields a 4.2σ deviation from the SM result predicted by the Theory Initiative White Paper (WP) [129] (based on refs. [130–149]). There is also a competing Lattice QCD prediction for the a_μ^{HVP} contribution from the BMW Collaboration [150] which results in only a 1.6σ

JHEP11(2022)139

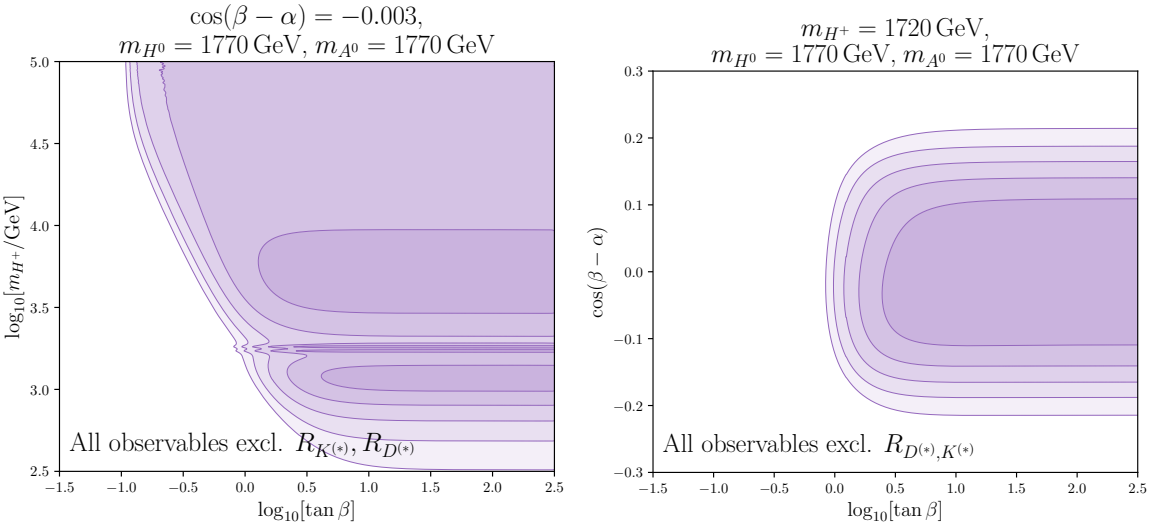

Figure 9. Combined fit of all flavour observables (excluding $R_{D^{(*)},K^{(*)}}$), Higgs signal strengths, and EWPOs in the 2HDM-I (in the $\tan\beta - m_{H^+}$ plane), fixing the additional parameters to their best-fit points. Contours are shown representing allowed parameter space at 1,2,3,4,5σ confidence from darkest to lightest.

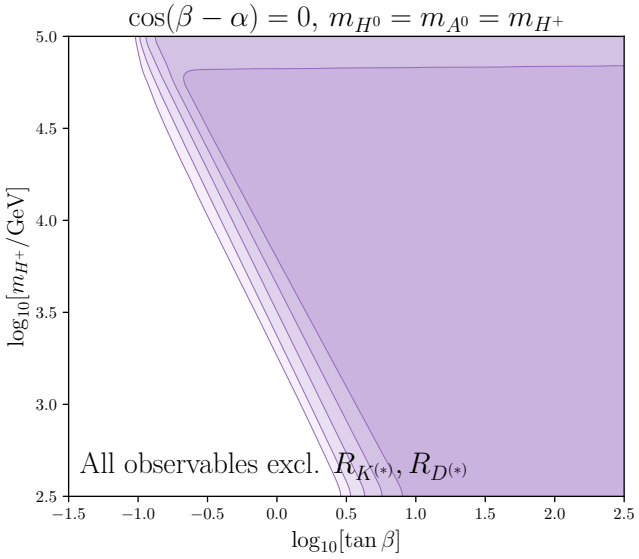

Figure 10. Combined fit of all flavour observables (excluding $R_{D^{(*)},K^{(*)}}$), Higgs signal strengths, and EWPOs in the 2HDM-I (in the $\tan\beta - m_{H^+}$ plane), taken in the limits of alignment ($\cos(\beta - \alpha) = 0$) and degenerate masses ($m_{H^0} = m_{A^0} = m_{H^+}$). Contours are shown representing allowed parameter space at 1,2,3,4,5σ confidence from darkest to lightest.

JHEP11(2022)139

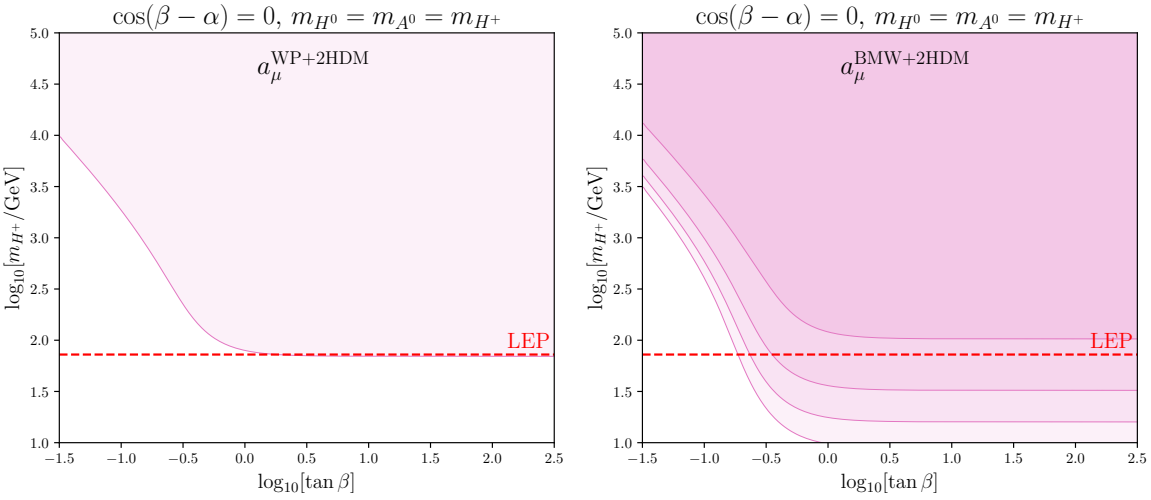

Figure 11. Contour plot of allowed 2HDM-I parameter space in the $(\tan\beta - m_{H^+})$ plane for a_μ, taken in the limits of alignment $(\cos(\beta-\alpha)=0)$ and degenerate masses $(m_{H^0}=m_{A^0}=m_{H^+})$. In the left plot, the SM prediction taken from the theory initiative is used; in the right, the SM result from the BMW collaboration. Contours are plotted representing allowed parameter space at 1,2,3,4,5σ confidence from darkest to lightest: in the left plot, only the 5σ contour is visible; in the right, the $2,3,4,5\sigma$ contours. The red dashed line indicates the LEP lower bound for m_{H^+} in the Type I 2HDM (72.5 GeV).

discrepancy from experiment.[4] Here, we fit a_μ to the 2HDM-I parameters considering both the WP and the BMW SM scenarios, shown in figure 11. We take the one- and two-loop contributions of the 2HDM to a_μ from ref. [67] where one can insert the expressions for the 2HDM-I couplings and we then convert the results to **flavio**'s WET-3 basis as described in section 7.2 of ref. [13]. As before, to present information in terms of two-dimensional fits, we fix the additional 2HDM parameters $\cos(\beta-\alpha)=0$ and $m_{H^+}=m_{H^0}=m_{A^0}$ as motivated by theory.

We find that in the 2HDM-I, a_μ strongly favours low $m_{H^+}\sim 100\,\text{MeV}$, low $\tan\beta\sim 0.5$, where the tension between experiment and theory using either SM prediction can be reduced to much less than 1σ. This result is however below the physical domain for m_{H^+}. Within the physical domain, we find that $m_{H^+}\gtrsim 100\,\text{GeV}$ can yield a tension between the WP and experiment of less than 5σ, with a minimum of 4.2σ, and between BMW and experiment less than a 2σ tension, with a minimum of 1.6σ.

5.4 2HDM-I and II flavour prospects at future colliders

Finally, we would like to discuss the prospects of the 2HDM flavour sector at future colliders. An approximate prediction for B-physics at future colliders such as the HL-LHC or beyond is that the precision of the measurements will roughly double from that of today's [160, 161]. With this in mind, we explore several scenarios for flavour observables in the future. Denoting the present-day experimental value of some observable as $M\pm E$, where M is the

[4]There are several lattice calculations [151–159] which were included in the WP, however the precision of these are much lower than either data-driven approach or the BMW calculation.

JHEP11(2022)139

central value and E the uncertainty, for each observable we now set $E \to E/2$ and consider 5 scenarios for a shift in M in the range $[M - E, M + E]$, where M for all observables shifts in the same way. We also consider an "Ideal" future scenario whereby M for each observable is individually shifted within $[M - E, M + E]$ to minimise its best-fit point χ^2 contribution; this scenario generally brings M to the SM prediction or as close as possible within $[M - E, M + E]$, and can be considered qualitatively similar to an extrapolation assuming the SM result.

We perform this process on ∼200 of our 275 observables which are identified as being "experimentally-limited" in their χ^2 contribution: that is, their present χ^2 contribution is dominated by the size of their experimental uncertainty. It is assumed in these tests that the theoretical calculations and precision do not change significantly by the time of these future measurements.

In table 4, we list the comparison of the χ^2 best fits in the SM, 2HDM-I, 2HDM-II for first the present situation and then each future scenario considered. We also list the lower bound of m_{H^+} from $\bar{B} \to X_s\gamma$ in the 2HDM-II for each scenario, as this has been an important bound in the history of the 2HDM and can remain so in the future. It is unlikely that any one of the exact scenarios would come to pass from future measurements for such a large group of observables, however comparison between all 6 scenarios sheds some light on the future suitability of the SM and the 2HDMs. In the present, we find that both the 2HDM-I and 2HDM-II perform better than the SM by $\sim 2\sigma$. In all future scenarios, the 2HDM-II still performs better than the SM, with a pull $> 1\sigma$ in all but one of these. The 2HDM-I's performance over the SM is narrowed significantly however, where the best future scenarios for this have a reduced pull of 1σ. In the "Ideal" future, the SM, 2HDM-I, and 2HDM-II all significantly improve upon their current positions; the majority of observables in this "Ideal" scenario simply move much closer to their SM predictions, where the small contributions from the 2HDMs either are not significant or are sufficient to improve upon the remaining small tensions with the SM.

Overall, it is found that increased precision of flavour observables at future colliders can lead to much poorer fits in both the SM and the 2HDM. The exception to this is when measurements are shifted much closer to the SM predictions and the small 2HDM contributions can be sufficient to resolve much of the remaining differences. While the future measurements' central values may not follow the scenarios considered here, the limiting factor in the χ^2 values in table 4 is the increased precision of measurements. Unless future measurements would indeed conform closely to our "Ideal" future scenario, the performances of the SM, 2HDM-I, 2HDM-II would all become very poor. While assuming no significant gaps in our theory predictions, this suggests some New Physics other than the 2HDM should be explored.

6 LHC constraints, flavour comparison and outlook

Having explored flavour constraints and their projections in detail in the previous section, we now turn to constraints from collider measurements of exotics searches. Such direct searches for Higgs bosons have a long history. Indeed, searching for the Higgs boson of the

JHEP11(2022)139

Scenario	SM	2HDM-I	2HDM-II	$\text{Min}(m_{H^+})^{b\to s\gamma}_{\text{2HDM-II}}, 2\sigma$
Present	292	281 ($+1.9\sigma$)	282 ($+1.8\sigma$)	790 GeV
"Ideal" future	174	169 ($+0.8\sigma$)	166 ($+1.4\sigma$)	680 GeV
$M \pm E/2$	721	717 ($+0.7\sigma$)	711 ($+1.7\sigma$)	940 GeV
$(M-E) \pm E/2$	811	808 ($+0.4\sigma$)	808 ($+0.4\sigma$)	1050 GeV
$(M-E/2) \pm E/2$	815	812 ($+0.4\sigma$)	804 ($+2.0\sigma$)	1000 GeV
$(M+E/2) \pm E/2$	896	891 ($+0.8\sigma$)	887 ($+1.6\sigma$)	680 GeV
$(M+E) \pm E/2$	899	893 ($+1.0\sigma$)	887 ($+2.1\sigma$)	770 GeV

	Best-fit point $\{\tan\beta, m_{H^+}, m_{H^0}, m_{A^0}, \cos(\beta-\alpha)\}$
2HDM-I	$\{80, 1720\,\text{GeV}, 1770\,\text{GeV}, 1770\,\text{GeV}, -0.003\}$
2HDM-II	$\{4.3, 2340\,\text{GeV}, 2380\,\text{GeV}, 2390\,\text{GeV}, 0.009\}$

Table 4. Summary of future prediction scenarios and their χ^2 best fits. For the 2HDMs in brackets are the pulls from the SM where a positive value indicates an improvement and a negative value a worsening. The results are shown for excluding $R_{D^{(*)},K^{(*)}}$. Also shown is the variation of the lower bound of the charged Higgs mass in the 2HDM-II from $\bar{B} \to X_s\gamma$.

SM was the raison d'être of the LHC, picking up where other colliders such as the LEP left off. In the years since the Higgs discovery, many precise measurements of the 125 GeV scalar have been made (see above), while searches for other, more exotic, Higgs bosons have continued alongside the precision measurements of the observed Higgs (see also refs. [162, 163]). These precision measurements closely match the phenomenology predicted of the SM Higgs. In this section we look to combine the wealth of experimental data on direct searches for new Higgs bosons to further constrain the allowed parameter space of the 2HDM, independently from the constraints in the prior sections, before combining these results in section 6.3. We also extrapolate the current LHC bounds to the expected results at the HL-LHC operating at 3 ab^{-1} in the same channels.

As in the rest of this work, the parameters of primary interest here are the masses of the new Higgs bosons and the angles $\tan\beta$ and $\cos(\beta-\alpha)$. Following the results of section 5.2, we examine the favoured scenario in which the new Higgs bosons have degenerate masses and the alignment limit holds.

6.1 Current collider bounds

In order to leverage the power of the vast array of search data we use the packages `HiggsBounds` [164–170] and `2HDecay` [171–176]. We use `2HDecay` to calculate the branching ratios and decay widths of each 2HDM Higgs boson for a given point in parameter space, and interface this data with `HiggsBounds` to check if the search data excludes such a point. For the key channel of H^+ production in association with $t\bar{b}$, we use `MadGraph5_aMC@NLO` [177] to generate cross sections which also form part of the input to `HiggsBounds`, along with the couplings of the Higgs bosons as given in table 2. We

JHEP11(2022)139

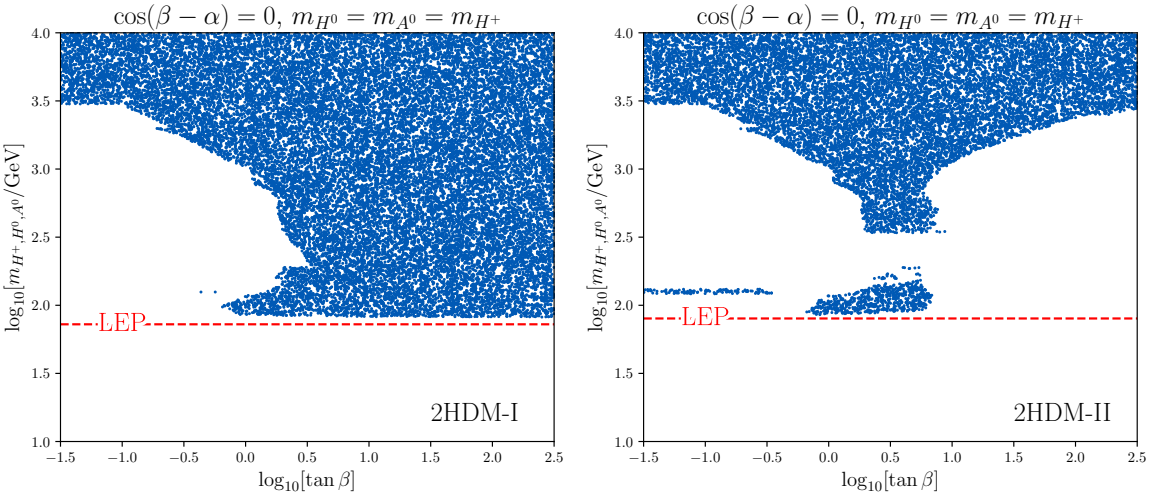

Figure 12. Scan of 50000 randomly generated points compared against LHC data using `2HDecay` and `HiggsBounds`, with allowed points shown in blue. On the left, the scan in the 2HDM-I, on the right the 2HDM-II.

perform scans using 50000 randomly generated points in the parameter space following this method and show the allowed points for both type I and II 2HDMs in figure 12. The historic baseline sensitivity from LEP [178] excludes charged Higgs masses below 72.5 GeV and 80 GeV for the Type I and Type II 2HDM models respectively, which we show as a dashed red line on each of the following figures.

In the 2HDM-I scan on the left of figure 12, at low values of $\tan\beta$, leptonic decays of the neutral Higgses (e.g. $H^0 \to \mu^+\mu^-$ in ref. [179]) exclude lower masses. Sensitivity to $H^+ \to \tau^+\nu_\tau$ peaks at $\sim 85\,\text{GeV}$ [180] and then the $H^+ \to t\bar{b}$ [181] decay provides the exclusion from $\sim 250\,\text{GeV}$ until falling cross sections lead to a loss of sensitivity at $\sim 2.5\,\text{TeV}$, beyond which points are allowed. This exclusion limit falls with increasing $\tan\beta$ as the H^+tb coupling is proportional to $\cot^2\beta$.[5] At moderate $\tan\beta$ the low mass exclusion limit shifts to $H^0/A^0 \to 4b$ [182]. The kink at $\sim 100\,\text{GeV}$ in the moderate $\tan\beta$ region is a result of $\mathcal{B}(H^+ \to \tau^+\nu_\tau)$ falling to zero as $\mathcal{B}(H^+ \to t\bar{b})$ rises to unity in this mass region, with $\mathcal{B}(H^+ \to t\bar{b}) \approx 1$ from $m_{H^\pm} \gtrsim m_t$. Sensitivity is lost from $H^0 \to \ell\ell$ as $\kappa_\ell^{H^0} \propto \cot\beta$, see table 2. The flat cut off at 80 GeV results from $H^+ \to qq/\tau^+\nu_\tau$ [178].

For the case of the 2HDM-II at low $\tan\beta$, $H^0 \to \gamma\gamma$ and $H^+ \to t\bar{b}$ compete to give the most stringent exclusion bounds [181, 183, 184], with $H^+ \to t\bar{b}$ being more sensitive at higher masses before the production cross sections fall at high masses. At moderate values of $\tan\beta$, $H^+ \to \tau^+\nu_\tau$ excludes masses up to $\sim 90\,\text{GeV}$, before the branching ratio for this channel falls, which leads to the allowed region at $\tan\beta$ of order 1 and masses of $\sim 100\,\text{GeV}$. This region is then ended by the $H^0 \to \tau^+\tau^-$ search in ref. [185]. This search also gives the exclusion up to high masses in the large $\tan\beta$ region, exceeding the limits from $H^+ \to t\bar{b}$.

We are able to find lower mass bounds on the new Higgs bosons of 82 GeV and 86 GeV in the Type I and II 2HDM respectively, which are less stringent bounds than those found

[5] The relevant Yukawa coupling is $2((m_t\xi^u_{H^+})^2 + (m_b\xi^d_{H^+})^2)/v^2$, where $\xi^{u,d}_{H^+} = \xi^{u,d}_A$ in table 2.

JHEP11(2022)139

from the combined fit to flavour observables in section 5.2. These bounds improve at low $\tan\beta$ in both models, and also at high $\tan\beta$ in the 2HDM-II, owing to the dependence of the couplings of these models to $\tan\beta$. This is in line with the patterns we see in the flavour sector, where these couplings are also crucial.

6.2 Collider outlook

Looking to the future, the LHC is due to be upgraded considerably, increasing the integrated luminosity to $\mathcal{L}_{\text{HL-LHC}} = 3\ \text{ab}^{-1}$. This will have a sizeable impact, making it significantly harder for new particles to remain hidden. Here, we extrapolate the LHC data currently in `HiggsBounds` to this new luminosity by scaling the limits by a factor $\sqrt{(\mathcal{L}_0/\mathcal{L}_{\text{HL-LHC}})}$ for a search with a reference luminosity $\mathcal{L}_0$. There are important caveats to this extrapolation. One such caveat is that a number of searches are designed to precisely measure the SM Higgs behaviour. In these cases we match the bounds to what would be expected of the SM Higgs, as here we have a 125 GeV scalar in the exact alignment limit, which exactly matches the phenomenology of the SM Higgs. We make use of the SM Higgs predictions of ref. [186] for this. Additionally, a number of searches included in `HiggsBounds` are from LHC run 1, during which the LHC operated at a centre of mass energy of $\sqrt{s} = 7 - 8\,\text{TeV}$, whilst the HL-LHC will operate at $\sqrt{s} = 13 - 14\,\text{TeV}$. We therefore need to reflect increased cross sections for these searches together with luminosity improvements (see also ref. [187]). We again make use of the results from ref. [186] to perform this extrapolation for SM Higgs searches. For BSM Higgs searches we use `MadGraph5_aMC@NLO` [177] to calculate the increase in the production cross sections at the higher centre of mass energy as a function of the BSM Higgs mass and scale the search data limits accordingly. We again perform a scan consisting of 50000 random points, the results of which are shown in figure 13, which includes the outline of the scan in figure 12 for ease of comparison.

The permitted parameter space for the 2HDM is reduced at the future collider, based on extrapolating existing searches. In the 2HDM-I case this effect is only apparent at low $\tan\beta$, as the sensitivity to new Higgs bosons is minimal at high $\tan\beta$ because the relevant couplings are proportional to $\cot^2\beta$. The lower limit in this region is from a LEP search [178], which we do not extrapolate here, hence the same cut off is present here as in figure 12. There is no such issue in the 2HDM-II, and we find that the bounds improve significantly at the HL-LHC, bringing the lower mass bound into competition with those found from flavour constraints in section 5.4, save for a small region with masses of $\approx 95\,\text{GeV}$ and $\tan\beta \approx 2$.

6.3 Comparison with flavour

In order to compare the bounds found above from collider searches to those we find from the flavour sector, we overlap results from both sections. No statistical combination between the two is attempted here as we do not use `HiggsBounds` to give a combined exclusion from all search data but only check if a point is excluded by any one individual search. We again present the results from the scenario in which all new Higgs bosons have degenerate masses and the alignment limit is exactly realised, meaning the combination presented

JHEP11(2022)139

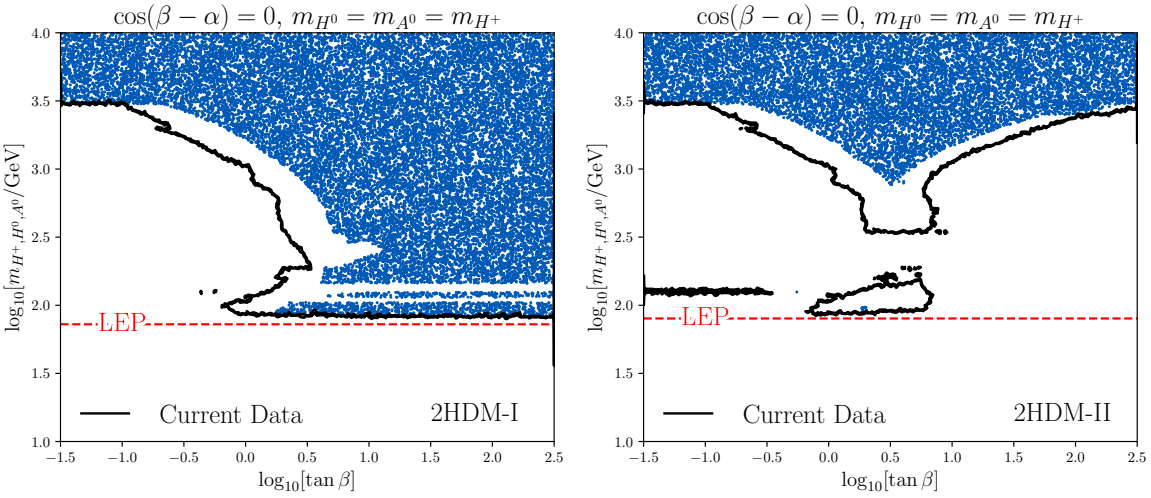

Figure 13. Scan of 50000 randomly generated points compared against LHC data, extrapolated to an integrated luminosity of 3 ab^{-1} using `2HDecay` and `HiggsBounds`, with allowed points shown in blue and the current data exclusion contour in black. On the left, the scan in the 2HDM-I, on the right the 2HDM-II.

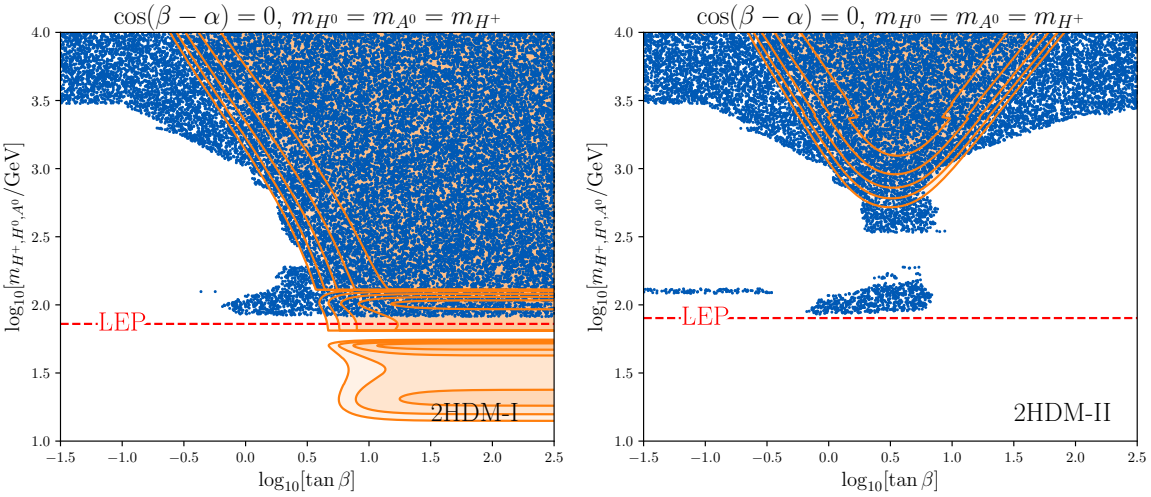

Figure 14. Combined results from the global flavour fit and collider searches, with allowed points from collider searches in blue and contours from the flavour sector at 1,2,3,4,5σ confidence, from darkest to lightest, with 2HDM-I results on the left and 2HDM-II on the right.

in figure 14 takes the results from figure 12 for collider results, and from figure 10 and the corresponding global fit in ref. [13] for flavour results, where we simply extend these contours to lower charged Higgs masses to be more compatible with the collider results.

We find that there is some degree of complementarity between the two sectors for the types of 2HDM that are examined here. In the 2HDM-I the LEP searches [178] that set a lower mass bound on the new Higgses outperform the exclusion from flavour observables, which lack sensitivity in the high $\tan\beta$ region. Conversely, in both cases, the flavour constraints following from precise measurements are more successful constraining $\tan\beta$

JHEP11(2022)139

at high masses, reflecting the loss of sensitivity in direct collider searches once the new particles are sufficiently heavy. Looking at the contours in figure 13, we can see that the extrapolation to the HL-LHC phase, which improves the sensitivity to new physics, enhances the complementary nature of the results in figure 14. In the case of the 2HDM-II the lower mass bound may exceed that determined from the flavour sector, depending on how future measurements in that sector line up with the scenarios outlined in section 5.4.

7 A note on cosmological context

As motivated by previous investigations [13, 15, 188–195], we consider the possibility of generating a strong first order electroweak phase transition (SFOEWPT) through the 2HDM-I in order to fulfil the criterion for EW baryogenesis. Scanning large parameter regions, these find possibilities for a SFOEWPT to be achieved in the 2HDM-I, however this is when considering lower masses ($\lesssim 1\,\text{TeV}$) than we find are favoured from our fits.

To evaluate the EWPT in the 2HDM-I at chosen benchmark points, we use the **BSMPT** package [196, 197], where we refer to the package's documentation[6] for further information on the package, and we make use of it as discussed in section 7.3 of ref. [13]. In table 5 we present the results for the strength of the EWPT at our selected parameter points. We first choose a benchmark of $M = 50\,\text{TeV}$ as a test of extreme masses, and then consider points motivated by our global fits in table 3 as well as some variation in $\tan\beta$. As the high masses of our best fits are suggested to be above the limit to achieve a SFOEWPT, we also consider a range of points with masses below 1 TeV, including the best fit point for the $b \to s\ell\ell$ observables. The alignment limit, $\cos(\beta - \alpha) = 0$, is taken for all benchmark points.

The results from these benchmark points are similar to those of the 2HDM-II. We find that the high mass scales around or above our best fit point (also enforcing close mass degeneracy) limit the strength of the phase transition. Sufficiently below our best fit points, where theoretical considerations now allow sampling with mass differences similar to those favoured in ref. [191], we now find scenarios which support a SFOEWPT. In contrast to the 2HDM-II, these points with $\xi_c \geq 1$ are each within 1σ confidence of our best fit and are allowed by direct search data. In these scenarios, the global fit performs only slightly worse than the best fit points described in table 3 with improvement over the SM at $\sim 1.5\sigma$.

8 Conclusions

The search for new physics beyond the Standard Model is key to improving our understanding of physics at the smallest distances. Searches at the LHC for new interactions and states have so far not revealed any significant deviation from the SM expectation, while the precision of flavour and electroweak precision measurements corner the SM from different directions with some potential hints for LFU violation.

In this work we have performed a detailed investigation and comparison of the flavour and LHC exotics measurement programme, alongside its future extrapolation. We find

[6] https://phbasler.github.io/BSMPT/.

JHEP11(2022)139

$\tan\beta$	Mass Basis (GeV)			Lambda Basis			m_{12}^2	ω_c	T_c	ξ_c
	m_{H^+}	m_{H^0}	m_{A^0}	λ_3	λ_4	λ_5	(GeV^2)	(GeV)	(GeV)	
11.4	50000	50000	50000	0.26	0	0	3.1×10^7	0.58	164	0.004
80	1750	1750	1750	0.26	0	0	3.8×10^4	23	162	0.14
50	1810	1750	1760	7.3	−6.5	−0.6	6.1×10^4	26	174	0.15
10	1810	1750	1760	7.3	−6.5	−0.6	3.0×10^5	26	174	0.15
150	1810	1750	1760	7.3	−6.5	−0.6	2.0×10^4	26	174	0.15
35	1020	960	970	4.2	−3.6	−0.3	2.6×10^4	24	169	0.14
80	860	710	860	8.0	−3.9	−3.9	6.3×10^3	142	174	0.82
80	860	690	860	9.0	−4.3	−4.3	6.0×10^3	177	174	1.02
80	680	470	680	8.2	−4.0	−4.0	2.8×10^3	211	147	1.43
80	570	320	570	7.6	−3.7	−3.7	1.3×10^3	226	125	1.81
80	490	250	490	6.1	−2.9	−2.9	7.8×10^2	207	126	1.65
80	490	490	490	0.26	0	0	3.0×10^3	23	161	0.14

Table 5. Table of results for the EWPT in the 2HDM-I. $\xi_c = \omega_c/T_c$ is the parameterisation of the strength of the EWPT, with ω_c the high-temperature VEV and T_c the critical temperature. A SFOEWPT is indicated by $\xi_c > 1$. In the limits chosen in ref. [13] (and similarly discussed in ref. [198]), $\lambda_1 = \lambda_2 = m_{h^0}^2/v^2 = 0.26$ for all benchmark points, and so are not explicitly shown in the table. Additionally, $\lambda_{3,4,5}$ are not independent, but $\lambda_3 + \lambda_4 + \lambda_5 = m_{h^0}^2/v^2 = 0.26$.

that both flavour and current exotics searches can be significantly improved with increasing luminosity, thus allowing the experimental collaborations to cover a significant proportion of parameter space that is currently unconstrained.

Extending the results of ref. [13] for 2HDM-II constraints from indirect searches using electroweak precision, Higgs signal strengths, and flavour observables to the type I 2HDM, we find that the 2HDM-I statistically outperforms both the 2HDM-II and the SM in fits to the data. The best fit point for the 2HDM-I lies around

$$\begin{aligned} &m_{H^+} \approx m_{H^0} \approx m_{A^0} \approx 1.7\,\text{TeV}\,, \\ &\tan\beta \approx 70, \qquad\qquad \cos(\beta-\alpha) \approx -0.001\,. \end{aligned} \tag{8.1}$$

The parameters of the 2HDM-I are found however to be much less constrained than in the 2HDM-II. An upper bound on the charged Higgs mass is only found at 1σ of 83 TeV, where for masses at or above ~ 1 TeV, the additional Higgses are expectedly to be closely degenerate. For a lower charged Higgs mass, $\tan\beta$ is strongly constrained from below to be $\mathcal{O}(1)$ or higher, however this constraint is lessened with increasing charged Higgs mass. The alignment limit, $\cos(\beta-\alpha) = 0$, is favoured by our fits, however larger deviations than in the 2HDM-II are allowed, up to $|\cos(\beta-\alpha)| = 0.4$ at 5σ.

Expecting an increase in precision of flavour measurements from future colliders, we consider our flavour fits in several future measurements' projections, where these predictive

JHEP11(2022)139

fits encourage consideration of other models instead of (or in addition to) a 2HDM of type I/II to improve upon the SM.

Furthermore, we consider the implications of these flavour fits on the electroweak phase transition of the early universe. It is found that the high masses encouraged by our fits do not support a strong EWPT for baryogenesis, however due to the 2HDM-I being less constrained than the 2HDM-II, sufficently low masses are possible within 1σ of our best fit.

Using data from direct searches for new fundamental particles at colliders we have been able to exclude large regions of the parameter space for the 2HDM of types I and II, highlighting possible areas to search for possible new physics. Looking forward, we have extrapolated a significant amount of data to match the expected performance of the HL-LHC and find that this further improves the constraints on new physics signals, to a level that can be competitive with indirect results from the flavour sector.

While some complementarity between flavour, Higgs physics and direct exotics searches remains, the finite energy coverage of exotics searches typically means a loss of direct LHC sensitivity for large masses approaching the decoupling limit.

Acknowledgments

O.A. is funded by a STFC studentship under grant ST/V506692/1. The work of M.B. is supported by Deutsche Forschungsgemeinschaft (DFG, German Research Foundation) through TRR 257 "Particle Physics Phenomenology after the Higgs Discovery". C.E. is supported by the STFC under grant ST/T000945/1, the Leverhulme Trust under grant RPG-2021-031, and the Institute for Particle Physics Phenomenology Associateship Scheme. Computations carried out for this work made use of the OMNI cluster of the University of Siegen.

References

[1] A.D. Sakharov, *Violation of CP Invariance, C asymmetry, and baryon asymmetry of the universe*, *Pisma Zh. Eksp. Teor. Fiz.* **5** (1967) 32 [INSPIRE].

[2] ATLAS collaboration, *Observation of a new particle in the search for the Standard Model Higgs boson with the ATLAS detector at the LHC*, *Phys. Lett. B* **716** (2012) 1 [arXiv:1207.7214] [INSPIRE].

[3] CMS collaboration, *Observation of a New Boson at a Mass of 125 GeV with the CMS Experiment at the LHC*, *Phys. Lett. B* **716** (2012) 30 [arXiv:1207.7235] [INSPIRE].

[4] F. Englert and R. Brout, *Broken Symmetry and the Mass of Gauge Vector Mesons*, *Phys. Rev. Lett.* **13** (1964) 321 [INSPIRE].

[5] P.W. Higgs, *Broken symmetries, massless particles and gauge fields*, *Phys. Lett.* **12** (1964) 132 [INSPIRE].

JHEP11(2022)139

[6] P.W. Higgs, *Broken Symmetries and the Masses of Gauge Bosons*, *Phys. Rev. Lett.* **13** (1964) 508 [INSPIRE].

[7] CMS collaboration, *Combination of searches for Higgs boson pair production in proton-proton collisions at $\sqrt{s} = 13$ TeV*, *Phys. Rev. Lett.* **122** (2019) 121803 [arXiv:1811.09689] [INSPIRE].

[8] ATLAS collaboration, *A combination of measurements of Higgs boson production and decay using up to 139 fb^{-1} of proton–proton collision data at $\sqrt{s} = 13$ TeV collected with the ATLAS experiment*, ATLAS-CONF-2020-027, CERN, Geneva (2020).

[9] GFITTER GROUP collaboration, *The global electroweak fit at NNLO and prospects for the LHC and ILC*, *Eur. Phys. J. C* **74** (2014) 3046 [arXiv:1407.3792] [INSPIRE].

[10] G.C. Branco, P.M. Ferreira, L. Lavoura, M.N. Rebelo, M. Sher and J.P. Silva, *Theory and phenomenology of two-Higgs-doublet models*, *Phys. Rept.* **516** (2012) 1 [arXiv:1106.0034] [INSPIRE].

[11] J.F. Gunion, H.E. Haber, G.L. Kane and S. Dawson, *The Higgs Hunter's Guide*, vol. 80, Perseus Publishing (2000).

[12] J.F. Gunion, R. Vega and J. Wudka, *Naturalness problems for rho = 1 and other large one loop effects for a standard model Higgs sector containing triplet fields*, *Phys. Rev. D* **43** (1991) 2322 [INSPIRE].

[13] O. Atkinson, M. Black, A. Lenz, A. Rusov and J. Wynne, *Cornering the Two Higgs Doublet Model Type II*, *JHEP* **04** (2022) 172 [arXiv:2107.05650] [INSPIRE].

[14] PARTICLE DATA GROUP collaboration, *Review of Particle Physics*, *PTEP* **2020** (2020) 083C01 [INSPIRE].

[15] P. Basler, M. Krause, M. Muhlleitner, J. Wittbrodt and A. Wlotzka, *Strong First Order Electroweak Phase Transition in the CP-Conserving 2HDM Revisited*, *JHEP* **02** (2017) 121 [arXiv:1612.04086] [INSPIRE].

[16] P. Arnan, D. Bečirević, F. Mescia and O. Sumensari, *Two Higgs doublet models and $b \to s$ exclusive decays*, *Eur. Phys. J. C* **77** (2017) 796 [arXiv:1703.03426] [INSPIRE].

[17] X.-F. Han and H.-X. Wang, *Revisiting wrong sign Yukawa coupling of type-II two-Higgs-doublet model in light of recent LHC data*, *Chin. Phys. C* **44** (2020) 073101 [arXiv:2003.06170] [INSPIRE].

[18] F. Kling, J.M. No and S. Su, *Anatomy of Exotic Higgs Decays in 2HDM*, *JHEP* **09** (2016) 093 [arXiv:1604.01406] [INSPIRE].

[19] A. Crivellin, D. Müller and C. Wiegand, *$b \to s\ell^+\ell^-$ transitions in two-Higgs-doublet models*, *JHEP* **06** (2019) 119 [arXiv:1903.10440] [INSPIRE].

[20] N. Chen, T. Han, S. Su, W. Su and Y. Wu, *Type-II 2HDM under the Precision Measurements at the Z-pole and a Higgs Factory*, *JHEP* **03** (2019) 023 [arXiv:1808.02037] [INSPIRE].

[21] I.F. Ginzburg and I.P. Ivanov, *Tree-level unitarity constraints in the most general 2HDM*, *Phys. Rev. D* **72** (2005) 115010 [hep-ph/0508020] [INSPIRE].

[22] B. Grinstein, C.W. Murphy and P. Uttayarat, *One-loop corrections to the perturbative unitarity bounds in the CP-conserving two-Higgs doublet model with a softly broken $\mathbb{Z}_2$ symmetry*, *JHEP* **06** (2016) 070 [arXiv:1512.04567] [INSPIRE].

JHEP11(2022)139

[23] V. Cacchio, D. Chowdhury, O. Eberhardt and C.W. Murphy, *Next-to-leading order unitarity fits in Two-Higgs-Doublet models with soft $\mathbb{Z}_2$ breaking*, *JHEP* **11** (2016) 026 [arXiv:1609.01290] [INSPIRE].

[24] N.G. Deshpande and E. Ma, *Pattern of Symmetry Breaking with Two Higgs Doublets*, *Phys. Rev. D* **18** (1978) 2574 [INSPIRE].

[25] A. Barroso, P.M. Ferreira, I.P. Ivanov and R. Santos, *Metastability bounds on the two Higgs doublet model*, *JHEP* **06** (2013) 045 [arXiv:1303.5098] [INSPIRE].

[26] A. Arhrib, *Unitarity constraints on scalar parameters of the standard and two Higgs doublets model*, in *Workshop on Noncommutative Geometry, Superstrings and Particle Physics*2000 [hep-ph/0012353] [INSPIRE].

[27] J. Horejsi and M. Kladiva, *Tree-unitarity bounds for THDM Higgs masses revisited*, *Eur. Phys. J. C* **46** (2006) 81 [hep-ph/0510154] [INSPIRE].

[28] M.E. Peskin and T. Takeuchi, *A New constraint on a strongly interacting Higgs sector*, *Phys. Rev. Lett.* **65** (1990) 964 [INSPIRE].

[29] M.E. Peskin and T. Takeuchi, *Estimation of oblique electroweak corrections*, *Phys. Rev. D* **46** (1992) 381 [INSPIRE].

[30] W. Grimus, L. Lavoura, O.M. Ogreid and P. Osland, *The Oblique parameters in multi-Higgs-doublet models*, *Nucl. Phys. B* **801** (2008) 81 [arXiv:0802.4353] [INSPIRE].

[31] R. Barbieri, A. Pomarol, R. Rattazzi and A. Strumia, *Electroweak symmetry breaking after LEP-1 and LEP-2*, *Nucl. Phys. B* **703** (2004) 127 [hep-ph/0405040] [INSPIRE].

[32] CMS collaboration, *Combined measurements of Higgs boson couplings in proton–proton collisions at $\sqrt{s} = 13$ TeV*, *Eur. Phys. J. C* **79** (2019) 421 [arXiv:1809.10733] [INSPIRE].

[33] CMS collaboration, *A search for the standard model Higgs boson decaying to charm quarks*, *JHEP* **03** (2020) 131 [arXiv:1912.01662] [INSPIRE].

[34] ATLAS collaboration, *Combined measurements of Higgs boson production and decay using up to 80 fb^{-1} of proton-proton collision data at $\sqrt{s} = 13$ TeV collected with the ATLAS experiment*, *Phys. Rev. D* **101** (2020) 012002 [arXiv:1909.02845] [INSPIRE].

[35] ATLAS collaboration, *A search for the $Z\gamma$ decay mode of the Higgs boson in pp collisions at $\sqrt{s} = 13$ TeV with the ATLAS detector*, *Phys. Lett. B* **809** (2020) 135754 [arXiv:2005.05382] [INSPIRE].

[36] ATLAS collaboration, *A search for the dimuon decay of the Standard Model Higgs boson with the ATLAS detector*, *Phys. Lett. B* **812** (2021) 135980 [arXiv:2007.07830] [INSPIRE].

[37] CMS collaboration, *Combined Higgs boson production and decay measurements with up to 137fb^{-1} of proton-proton collision data at $\sqrt{s} = 13$ TeV*, CMS-PAS-HIG-19-005, CERN, Geneva (2020).

[38] CMS collaboration, *Measurements of Higgs boson production cross sections and couplings in the diphoton decay channel at $\sqrt{s} = 13$ TeV*, *JHEP* **07** (2021) 027 [arXiv:2103.06956] [INSPIRE].

[39] ATLAS collaboration, *Measurements of gluon fusion and vector-boson-fusion production of the Higgs boson in $H \to WW^* \to e\nu\mu\nu$ decays using pp collisions at $\sqrt{s} = 13$ TeV with the ATLAS detector*, ATLAS-CONF-2021-014, CERN, Geneva (2021).

JHEP11(2022)139

[40] CMS collaboration, *Evidence for Higgs boson decay to a pair of muons*, *JHEP* **01** (2021) 148 [arXiv:2009.04363] [INSPIRE].

[41] ATLAS collaboration, *Measurements of Higgs bosons decaying to bottom quarks from vector boson fusion production with the ATLAS experiment at* $\sqrt{s} = 13$ *TeV*, *Eur. Phys. J. C* **81** (2021) 537 [arXiv:2011.08280] [INSPIRE].

[42] ATLAS collaboration, *Measurements of* WH *and* ZH *production in the* $H \to b\bar{b}$ *decay channel in pp collisions at 13 TeV with the ATLAS detector*, *Eur. Phys. J. C* **81** (2021) 178 [arXiv:2007.02873] [INSPIRE].

[43] HFLAV collaboration, *Averages of b-hadron, c-hadron, and* τ*-lepton properties as of 2018*, *Eur. Phys. J. C* **81** (2021) 226 [arXiv:1909.12524] [INSPIRE].

[44] LHCb collaboration, *Measurement of* $|V_{cb}|$ *with* $B_s^0 \to D_s^{(*)-}\mu^+\nu_\mu$ *decays*, *Phys. Rev. D* **101** (2020) 072004 [arXiv:2001.03225] [INSPIRE].

[45] LHCb collaboration, *Precise measurement of the* f_s/f_d *ratio of fragmentation fractions and of* B_s^0 *decay branching fractions*, *Phys. Rev. D* **104** (2021) 032005 [arXiv:2103.06810] [INSPIRE].

[46] E. McLean, C.T.H. Davies, J. Koponen and A.T. Lytle, $B_s \to D_s\ell\nu$ *Form Factors for the full* q^2 *range from Lattice QCD with non-perturbatively normalized currents*, *Phys. Rev. D* **101** (2020) 074513 [arXiv:1906.00701] [INSPIRE].

[47] W. Altmannshofer and P. Stangl, *New physics in rare B decays after Moriond 2021*, *Eur. Phys. J. C* **81** (2021) 952 [arXiv:2103.13370] [INSPIRE].

[48] LHCb collaboration, *Differential branching fractions and isospin asymmetries of* $B \to K^{(*)}\mu^+\mu^-$ *decays*, *JHEP* **06** (2014) 133 [arXiv:1403.8044] [INSPIRE].

[49] LHCb collaboration, *Angular Analysis of the* $B^+ \to K^{*+}\mu^+\mu^-$ *Decay*, *Phys. Rev. Lett.* **126** (2021) 161802 [arXiv:2012.13241] [INSPIRE].

[50] LHCb collaboration, *Measurement of CP-Averaged Observables in the* $B^0 \to K^{*0}\mu^+\mu^-$ *Decay*, *Phys. Rev. Lett.* **125** (2020) 011802 [arXiv:2003.04831] [INSPIRE].

[51] ATLAS collaboration, *Angular analysis of* $B_d^0 \to K^*\mu^+\mu^-$ *decays in pp collisions at* $\sqrt{s} = 8$ *TeV with the ATLAS detector*, *JHEP* **10** (2018) 047 [arXiv:1805.04000] [INSPIRE].

[52] CMS collaboration, *Angular analysis of the decay* $B^0 \to K^{*0}\mu^+\mu^-$ *from pp collisions at* $\sqrt{s} = 8$ *TeV*, *Phys. Lett. B* **753** (2016) 424 [arXiv:1507.08126] [INSPIRE].

[53] CMS collaboration, *Measurement of angular parameters from the decay* $\mathrm{B}^0 \to \mathrm{K}^{*0}\mu^+\mu^-$ *in proton-proton collisions at* $\sqrt{s} = 8$ *TeV*, *Phys. Lett. B* **781** (2018) 517 [arXiv:1710.02846] [INSPIRE].

[54] BELLE collaboration, *Test of lepton flavor universality and search for lepton flavor violation in* $B \to K\ell\ell$ *decays*, *JHEP* **03** (2021) 105 [arXiv:1908.01848] [INSPIRE].

[55] BELLE collaboration, *Test of Lepton-Flavor Universality in* $B \to K^*\ell^+\ell^-$ *Decays at Belle*, *Phys. Rev. Lett.* **126** (2021) 161801 [arXiv:1904.02440] [INSPIRE].

[56] LHCb collaboration, *Angular analysis and differential branching fraction of the decay* $B_s^0 \to \phi\mu^+\mu^-$, *JHEP* **09** (2015) 179 [arXiv:1506.08777] [INSPIRE].

[57] BABAR collaboration, *Measurement of the* $B \to X_s l^+ l^-$ *branching fraction and search for direct CP-violation from a sum of exclusive final states*, *Phys. Rev. Lett.* **112** (2014) 211802 [arXiv:1312.5364] [INSPIRE].

JHEP11(2022)139

[58] Belle collaboration, *Lepton-Flavor-Dependent Angular Analysis of $B \to K^* \ell^+ \ell^-$*, *Phys. Rev. Lett.* **118** (2017) 111801 [arXiv:1612.05014] [INSPIRE].

[59] LHCb collaboration, *Angular analysis of the $B^0 \to K^{*0} e^+ e^-$ decay in the low-q^2 region*, *JHEP* **04** (2015) 064 [arXiv:1501.03038] [INSPIRE].

[60] CMS collaboration, *Angular analysis of the decay $B^+ \to K^+ \mu^+ \mu^-$ in proton-proton collisions at $\sqrt{s} = 8$ TeV*, *Phys. Rev. D* **98** (2018) 112011 [arXiv:1806.00636] [INSPIRE].

[61] LHCb collaboration, *Differential branching fraction and angular analysis of $\Lambda_b^0 \to \Lambda \mu^+ \mu^-$ decays*, *JHEP* **06** (2015) 115 [*Erratum ibid.* **09** (2018) 145] [arXiv:1503.07138] [INSPIRE].

[62] LHCb collaboration, *Angular moments of the decay $\Lambda_b^0 \to \Lambda \mu^+ \mu^-$ at low hadronic recoil*, *JHEP* **09** (2018) 146 [arXiv:1808.00264] [INSPIRE].

[63] LHCb collaboration, *Test of lepton universality in beauty-quark decays*, *Nature Phys.* **18** (2022) 277 [arXiv:2103.11769] [INSPIRE].

[64] LHCb collaboration, *Test of lepton universality using $B^+ \to K^+ \ell^+ \ell^-$ decays*, *Phys. Rev. Lett.* **113** (2014) 151601 [arXiv:1406.6482] [INSPIRE].

[65] LHCb collaboration, *Test of lepton universality with $B^0 \to K^{*0} \ell^+ \ell^-$ decays*, *JHEP* **08** (2017) 055 [arXiv:1705.05802] [INSPIRE].

[66] BaBar collaboration, *Measurement of Branching Fractions and Rate Asymmetries in the Rare Decays $B \to K^{(*)} l^+ l^-$*, *Phys. Rev. D* **86** (2012) 032012 [arXiv:1204.3933] [INSPIRE].

[67] V. Ilisie, *New Barr-Zee contributions to $(\mathbf{g-2})_\mu$ in two-Higgs-doublet models*, *JHEP* **04** (2015) 077 [arXiv:1502.04199] [INSPIRE].

[68] F. Borzumati and C. Greub, *2HDMs predictions for $\bar{B} \to X(s)\gamma$ in NLO QCD*, *Phys. Rev. D* **58** (1998) 074004 [hep-ph/9802391] [INSPIRE].

[69] F. Borzumati and C. Greub, *Two Higgs doublet model predictions for $\bar{B} \to X(s)\gamma$ in NLO QCD: Addendum*, *Phys. Rev. D* **59** (1999) 057501 [hep-ph/9809438] [INSPIRE].

[70] F.U. Bernlochner, Z. Ligeti, M. Papucci and D.J. Robinson, *Combined analysis of semileptonic B decays to D and D^*: $R(D^{(*)})$, $|V_{cb}|$, and new physics*, *Phys. Rev. D* **95** (2017) 115008 [*Erratum ibid.* **97** (2018) 059902] [arXiv:1703.05330] [INSPIRE].

[71] I. Caprini, L. Lellouch and M. Neubert, *Dispersive bounds on the shape of $\bar{B} \to D(*)$ lepton anti-neutrino form-factors*, *Nucl. Phys. B* **530** (1998) 153 [hep-ph/9712417] [INSPIRE].

[72] Y. Sakaki, M. Tanaka, A. Tayduganov and R. Watanabe, *Testing leptoquark models in $\bar{B} \to D^{(*)} \tau \bar{\nu}$*, *Phys. Rev. D* **88** (2013) 094012 [arXiv:1309.0301] [INSPIRE].

[73] A. Bharucha, D.M. Straub and R. Zwicky, *$B \to V \ell^+ \ell^-$ in the Standard Model from light-cone sum rules*, *JHEP* **08** (2016) 098 [arXiv:1503.05534] [INSPIRE].

[74] N. Gubernari, A. Kokulu and D. van Dyk, *$B \to P$ and $B \to V$ Form Factors from B-Meson Light-Cone Sum Rules beyond Leading Twist*, *JHEP* **01** (2019) 150 [arXiv:1811.00983] [INSPIRE].

[75] W. Detmold and S. Meinel, *$\Lambda_b \to \Lambda \ell^+ \ell^-$ form factors, differential branching fraction, and angular observables from lattice QCD with relativistic b quarks*, *Phys. Rev. D* **93** (2016) 074501 [arXiv:1602.01399] [INSPIRE].

[76] V. Bernard, M. Oertel, E. Passemar and J. Stern, *K(mu3)**L decay: A Stringent test of right-handed quark currents*, *Phys. Lett. B* **638** (2006) 480 [hep-ph/0603202] [INSPIRE].

JHEP11(2022)139

[77] V. Bernard, M. Oertel, E. Passemar and J. Stern, *Dispersive representation and shape of the K(l3) form factors: Robustness*, *Phys. Rev. D* **80** (2009) 034034 [arXiv:0903.1654] [INSPIRE].

[78] FLAVIANET WORKING GROUP ON KAON DECAYS collaborations, *An Evaluation of $|V_{us}|$ and precise tests of the Standard Model from world data on leptonic and semileptonic kaon decays*, *Eur. Phys. J. C* **69** (2010) 399 [arXiv:1005.2323] [INSPIRE].

[79] L. Di Luzio, M. Kirk, A. Lenz and T. Rauh, *ΔM_s theory precision confronts flavour anomalies*, *JHEP* **12** (2019) 009 [arXiv:1909.11087] [INSPIRE].

[80] D. King, A. Lenz and T. Rauh, *B_s mixing observables and $|V_{td}/V_{ts}|$ from sum rules*, *JHEP* **05** (2019) 034 [arXiv:1904.00940] [INSPIRE].

[81] M. Kirk, A. Lenz and T. Rauh, *Dimension-six matrix elements for meson mixing and lifetimes from sum rules*, *JHEP* **12** (2017) 068 [*Erratum ibid.* **06** (2020) 162] [arXiv:1711.02100] [INSPIRE].

[82] A.G. Grozin, R. Klein, T. Mannel and A.A. Pivovarov, *$B^0 - \bar{B}^0$ mixing at next-to-leading order*, *Phys. Rev. D* **94** (2016) 034024 [arXiv:1606.06054] [INSPIRE].

[83] R.J. Dowdall et al., *Neutral B-meson mixing from full lattice QCD at the physical point*, *Phys. Rev. D* **100** (2019) 094508 [arXiv:1907.01025] [INSPIRE].

[84] RBC/UKQCD collaboration, *SU(3)-breaking ratios for $D_{(s)}$ and $B_{(s)}$ mesons*, arXiv:1812.08791 [INSPIRE].

[85] FERMILAB LATTICE, MILC collaborations, *$B^0_{(s)}$-mixing matrix elements from lattice QCD for the Standard Model and beyond*, *Phys. Rev. D* **93** (2016) 113016 [arXiv:1602.03560] [INSPIRE].

[86] M. Misiak, A. Rehman and M. Steinhauser, *Towards $\overline{B} \to X_s\gamma$ at the NNLO in QCD without interpolation in m_c*, *JHEP* **06** (2020) 175 [arXiv:2002.01548] [INSPIRE].

[87] M. Misiak and M. Steinhauser, *NNLO QCD corrections to the $\bar{B} \to X(s)\gamma$ matrix elements using interpolation in m(c)*, *Nucl. Phys. B* **764** (2007) 62 [hep-ph/0609241] [INSPIRE].

[88] M. Misiak et al., *Updated NNLO QCD predictions for the weak radiative B-meson decays*, *Phys. Rev. Lett.* **114** (2015) 221801 [arXiv:1503.01789] [INSPIRE].

[89] CLEO collaboration, *Branching fraction and photon energy spectrum for $b \to s\gamma$*, *Phys. Rev. Lett.* **87** (2001) 251807 [hep-ex/0108032] [INSPIRE].

[90] BABAR collaboration, *Precision Measurement of the $B \to X_s\gamma$ Photon Energy Spectrum, Branching Fraction, and Direct CP Asymmetry $A_{CP}(B \to X_{s+d}\gamma)$*, *Phys. Rev. Lett.* **109** (2012) 191801 [arXiv:1207.2690] [INSPIRE].

[91] BELLE collaboration, *Measurement of the inclusive $B \to X_{s+d}\gamma$ branching fraction, photon energy spectrum and HQE parameters*, in *38th International Conference on High Energy Physics*2016 [arXiv:1608.02344] [INSPIRE].

[92] LHCb collaboration, *Measurement of the $B^0_s \to \mu^+\mu^-$ branching fraction and effective lifetime and search for $B^0 \to \mu^+\mu^-$ decays*, *Phys. Rev. Lett.* **118** (2017) 191801 [arXiv:1703.05747] [INSPIRE].

[93] ATLAS collaboration, *Study of the rare decays of B^0_s and B^0 mesons into muon pairs using data collected during 2015 and 2016 with the ATLAS detector*, *JHEP* **04** (2019) 098 [arXiv:1812.03017] [INSPIRE].

JHEP11(2022)139

[94] CMS collaboration, *Measurement of properties of $B_s^0 \to \mu^+\mu^-$ decays and search for $B^0 \to \mu^+\mu^-$ with the CMS experiment*, *JHEP* **04** (2020) 188 [arXiv:1910.12127] [INSPIRE].

[95] CMS, LHCb, ATLAS collaborations, *Combination of the ATLAS, CMS and LHCb results on the $B^0_{(s)} \to \mu^+\mu^-$ decays*, CMS-PAS-BPH-20-003, LHCb-CONF-2020-002, ATLAS-CONF-2020-049, CERN, Geneva (2020).

[96] LHCb collaboration, *Measurement of the $B_s^0 \to \mu^+\mu^-$ decay properties and search for the $B^0 \to \mu^+\mu^-$ and $B_s^0 \to \mu^+\mu^-\gamma$ decays*, *Phys. Rev. D* **105** (2022) 012010 [arXiv:2108.09283] [INSPIRE].

[97] LHCb collaboration, *Analysis of Neutral B-Meson Decays into Two Muons*, *Phys. Rev. Lett.* **128** (2022) 041801 [arXiv:2108.09284] [INSPIRE].

[98] G. Buchalla and A.J. Buras, *QCD corrections to rare K and B decays for arbitrary top quark mass*, *Nucl. Phys. B* **400** (1993) 225 [INSPIRE].

[99] C. Bobeth, M. Gorbahn, T. Hermann, M. Misiak, E. Stamou and M. Steinhauser, *$B_{s,d} \to l^+l^-$ in the Standard Model with Reduced Theoretical Uncertainty*, *Phys. Rev. Lett.* **112** (2014) 101801 [arXiv:1311.0903] [INSPIRE].

[100] M. Beneke, C. Bobeth and R. Szafron, *Power-enhanced leading-logarithmic QED corrections to $B_q \to \mu^+\mu^-$*, *JHEP* **10** (2019) 232 [arXiv:1908.07011] [INSPIRE].

[101] ETM collaboration, *Mass of the b quark and B -meson decay constants from N_f=2+1+1 twisted-mass lattice QCD*, *Phys. Rev. D* **93** (2016) 114505 [arXiv:1603.04306] [INSPIRE].

[102] A. Bazavov et al., *B- and D-meson leptonic decay constants from four-flavor lattice QCD*, *Phys. Rev. D* **98** (2018) 074512 [arXiv:1712.09262] [INSPIRE].

[103] C. Hughes, C.T.H. Davies and C.J. Monahan, *New methods for B meson decay constants and form factors from lattice NRQCD*, *Phys. Rev. D* **97** (2018) 054509 [arXiv:1711.09981] [INSPIRE].

[104] C. Bobeth, G. Hiller and G. Piranishvili, *Angular distributions of $\bar{B} \to \bar{K}\ell^+\ell^-$ decays*, *JHEP* **12** (2007) 040 [arXiv:0709.4174] [INSPIRE].

[105] M. Bordone, G. Isidori and A. Pattori, *On the Standard Model predictions for R_K and R_{K^*}*, *Eur. Phys. J. C* **76** (2016) 440 [arXiv:1605.07633] [INSPIRE].

[106] T. Hurth, F. Mahmoudi and S. Neshatpour, *Model independent analysis of the angular observables in $B^0 \to K^{*0}\mu^+\mu^-$ and $B^+ \to K^{*+}\mu^+\mu^-$*, *Phys. Rev. D* **103** (2021) 095020 [arXiv:2012.12207] [INSPIRE].

[107] L.-S. Geng, B. Grinstein, S. Jäger, J. Martin Camalich, X.-L. Ren and R.-X. Shi, *Towards the discovery of new physics with lepton-universality ratios of $b \to s\ell\ell$ decays*, *Phys. Rev. D* **96** (2017) 093006 [arXiv:1704.05446] [INSPIRE].

[108] M. Ciuchini et al., *New Physics in $b \to s\ell^+\ell^-$ confronts new data on Lepton Universality*, *Eur. Phys. J. C* **79** (2019) 719 [arXiv:1903.09632] [INSPIRE].

[109] A. Datta, J. Kumar and D. London, *The B anomalies and new physics in $b \to se^+e^-$*, *Phys. Lett. B* **797** (2019) 134858 [arXiv:1903.10086] [INSPIRE].

[110] K. Kowalska, D. Kumar and E.M. Sessolo, *Implications for new physics in $b \to s\mu\mu$ transitions after recent measurements by Belle and LHCb*, *Eur. Phys. J. C* **79** (2019) 840 [arXiv:1903.10932] [INSPIRE].

JHEP11(2022)139

[111] T. Hurth, F. Mahmoudi and S. Neshatpour, *Implications of the new LHCb angular analysis of $B \to K^* \mu^+ \mu^-$: Hadronic effects or new physics?*, *Phys. Rev. D* **102** (2020) 055001 [arXiv:2006.04213] [INSPIRE].

[112] M. Ciuchini, M. Fedele, E. Franco, A. Paul, L. Silvestrini and M. Valli, *Lessons from the $B^{0,+} \to K^{*0,+} \mu^+ \mu^-$ angular analyses*, *Phys. Rev. D* **103** (2021) 015030 [arXiv:2011.01212] [INSPIRE].

[113] M. Algueró et al., *Emerging patterns of New Physics with and without Lepton Flavour Universal contributions*, *Eur. Phys. J. C* **79** (2019) 714 [*Addendum ibid.* **80** (2020) 511] [arXiv:1903.09578] [INSPIRE].

[114] A.K. Alok, A. Dighe, S. Gangal and D. Kumar, *Continuing search for new physics in $b \to s\mu\mu$ decays: two operators at a time*, *JHEP* **06** (2019) 089 [arXiv:1903.09617] [INSPIRE].

[115] J. Aebischer, W. Altmannshofer, D. Guadagnoli, M. Reboud, P. Stangl and D.M. Straub, *B-decay discrepancies after Moriond 2019*, *Eur. Phys. J. C* **80** (2020) 252 [arXiv:1903.10434] [INSPIRE].

[116] W. Altmannshofer, P. Stangl and D.M. Straub, *Interpreting Hints for Lepton Flavor Universality Violation*, *Phys. Rev. D* **96** (2017) 055008 [arXiv:1704.05435] [INSPIRE].

[117] A. Carvunis, F. Dettori, S. Gangal, D. Guadagnoli and C. Normand, *On the effective lifetime of $B_s \to \mu\mu\gamma$*, *JHEP* **12** (2021) 078 [arXiv:2102.13390] [INSPIRE].

[118] A. Khodjamirian, T. Mannel, A.A. Pivovarov and Y.M. Wang, *Charm-loop effect in $B \to K^{(*)} \ell^+ \ell^-$ and $B \to K^* \gamma$*, *JHEP* **09** (2010) 089 [arXiv:1006.4945] [INSPIRE].

[119] A. Khodjamirian, T. Mannel and Y.M. Wang, *$B \to K \ell^+ \ell^-$ decay at large hadronic recoil*, *JHEP* **02** (2013) 010 [arXiv:1211.0234] [INSPIRE].

[120] A. Khodjamirian and A.V. Rusov, *$B_s \to K \ell \nu_\ell$ and $B_{(s)} \to \pi(K) \ell^+ \ell^-$ decays at large recoil and CKM matrix elements*, *JHEP* **08** (2017) 112 [arXiv:1703.04765] [INSPIRE].

[121] T. Hurth, F. Mahmoudi, D.M. Santos and S. Neshatpour, *More Indications for Lepton Nonuniversality in $b \to s \ell^+ \ell^-$*, *Phys. Lett. B* **824** (2022) 136838 [arXiv:2104.10058] [INSPIRE].

[122] M. Algueró, B. Capdevila, S. Descotes-Genon, J. Matias and M. Novoa-Brunet, *$b \to s \ell^+ \ell^-$ global fits after R_{K_S} and $R_{K^{*+}}$*, *Eur. Phys. J. C* **82** (2022) 326 [arXiv:2104.08921] [INSPIRE].

[123] C. Cornella, D.A. Faroughy, J. Fuentes-Martin, G. Isidori and M. Neubert, *Reading the footprints of the B-meson flavor anomalies*, *JHEP* **08** (2021) 050 [arXiv:2103.16558] [INSPIRE].

[124] L.-S. Geng, B. Grinstein, S. Jäger, S.-Y. Li, J. Martin Camalich and R.-X. Shi, *Implications of new evidence for lepton-universality violation in $b \to s\ell+\ell-$ decays*, *Phys. Rev. D* **104** (2021) 035029 [arXiv:2103.12738] [INSPIRE].

[125] F. Munir Bhutta, Z.-R. Huang, C.-D. Lü, M.A. Paracha and W. Wang, *New physics in $b \to s\ell\ell$ anomalies and its implications for the complementary neutral current decays*, *Nucl. Phys. B* **979** (2022) 115763 [arXiv:2009.03588] [INSPIRE].

[126] A. Biswas, S. Nandi, S.K. Patra and I. Ray, *New physics in $b \to \ell\ell$ decays with complex Wilson coefficients*, *Nucl. Phys. B* **969** (2021) 115479 [arXiv:2004.14687] [INSPIRE].

JHEP11(2022)139

[127] Muon g-2 collaboration, *Measurement of the Positive Muon Anomalous Magnetic Moment to 0.46 ppm*, *Phys. Rev. Lett.* **126** (2021) 141801 [arXiv:2104.03281] [INSPIRE].

[128] Muon g-2 collaboration, *Final Report of the Muon E821 Anomalous Magnetic Moment Measurement at BNL*, *Phys. Rev. D* **73** (2006) 072003 [hep-ex/0602035] [INSPIRE].

[129] T. Aoyama et al., *The anomalous magnetic moment of the muon in the Standard Model*, *Phys. Rept.* **887** (2020) 1 [arXiv:2006.04822] [INSPIRE].

[130] T. Aoyama, M. Hayakawa, T. Kinoshita and M. Nio, *Complete Tenth-Order QED Contribution to the Muon g-2*, *Phys. Rev. Lett.* **109** (2012) 111808 [arXiv:1205.5370] [INSPIRE].

[131] T. Aoyama, T. Kinoshita and M. Nio, *Theory of the Anomalous Magnetic Moment of the Electron*, *Atoms* **7** (2019) 28 [INSPIRE].

[132] A. Czarnecki, W.J. Marciano and A. Vainshtein, *Refinements in electroweak contributions to the muon anomalous magnetic moment*, *Phys. Rev. D* **67** (2003) 073006 [*Erratum ibid.* **73** (2006) 119901] [hep-ph/0212229] [INSPIRE].

[133] C. Gnendiger, D. Stöckinger and H. Stöckinger-Kim, *The electroweak contributions to* $(g-2)_\mu$ *after the Higgs boson mass measurement*, *Phys. Rev. D* **88** (2013) 053005 [arXiv:1306.5546] [INSPIRE].

[134] M. Davier, A. Hoecker, B. Malaescu and Z. Zhang, *Reevaluation of the hadronic vacuum polarisation contributions to the Standard Model predictions of the muon* $g-2$ *and* $\alpha(m_Z^2)$ *using newest hadronic cross-section data*, *Eur. Phys. J. C* **77** (2017) 827 [arXiv:1706.09436] [INSPIRE].

[135] A. Keshavarzi, D. Nomura and T. Teubner, *Muon* $g-2$ *and* $\alpha(M_Z^2)$*: a new data-based analysis*, *Phys. Rev. D* **97** (2018) 114025 [arXiv:1802.02995] [INSPIRE].

[136] G. Colangelo, M. Hoferichter and P. Stoffer, *Two-pion contribution to hadronic vacuum polarization*, *JHEP* **02** (2019) 006 [arXiv:1810.00007] [INSPIRE].

[137] M. Hoferichter, B.-L. Hoid and B. Kubis, *Three-pion contribution to hadronic vacuum polarization*, *JHEP* **08** (2019) 137 [arXiv:1907.01556] [INSPIRE].

[138] M. Davier, A. Hoecker, B. Malaescu and Z. Zhang, *A new evaluation of the hadronic vacuum polarisation contributions to the muon anomalous magnetic moment and to* $\boldsymbol{\alpha(m_Z^2)}$, *Eur. Phys. J. C* **80** (2020) 241 [*Erratum ibid.* **80** (2020) 410] [arXiv:1908.00921] [INSPIRE].

[139] A. Keshavarzi, D. Nomura and T. Teubner, $g-2$ *of charged leptons,* $\alpha(M_Z^2)$ *, and the hyperfine splitting of muonium*, *Phys. Rev. D* **101** (2020) 014029 [arXiv:1911.00367] [INSPIRE].

[140] A. Kurz, T. Liu, P. Marquard and M. Steinhauser, *Hadronic contribution to the muon anomalous magnetic moment to next-to-next-to-leading order*, *Phys. Lett. B* **734** (2014) 144 [arXiv:1403.6400] [INSPIRE].

[141] K. Melnikov and A. Vainshtein, *Hadronic light-by-light scattering contribution to the muon anomalous magnetic moment revisited*, *Phys. Rev. D* **70** (2004) 113006 [hep-ph/0312226] [INSPIRE].

[142] P. Masjuan and P. Sanchez-Puertas, *Pseudoscalar-pole contribution to the* $(g_\mu-2)$*: a rational approach*, *Phys. Rev. D* **95** (2017) 054026 [arXiv:1701.05829] [INSPIRE].

JHEP11(2022)139

[143] G. Colangelo, M. Hoferichter, M. Procura and P. Stoffer, *Dispersion relation for hadronic light-by-light scattering: two-pion contributions*, *JHEP* **04** (2017) 161 [arXiv:1702.07347] [INSPIRE].

[144] M. Hoferichter, B.-L. Hoid, B. Kubis, S. Leupold and S.P. Schneider, *Dispersion relation for hadronic light-by-light scattering: pion pole*, *JHEP* **10** (2018) 141 [arXiv:1808.04823] [INSPIRE].

[145] A. Gérardin, H.B. Meyer and A. Nyffeler, *Lattice calculation of the pion transition form factor with $N_f = 2 + 1$ Wilson quarks*, *Phys. Rev. D* **100** (2019) 034520 [arXiv:1903.09471] [INSPIRE].

[146] J. Bijnens, N. Hermansson-Truedsson and A. Rodríguez-Sánchez, *Short-distance constraints for the HLbL contribution to the muon anomalous magnetic moment*, *Phys. Lett. B* **798** (2019) 134994 [arXiv:1908.03331] [INSPIRE].

[147] G. Colangelo, F. Hagelstein, M. Hoferichter, L. Laub and P. Stoffer, *Longitudinal short-distance constraints for the hadronic light-by-light contribution to $(g-2)_\mu$ with large-N_c Regge models*, *JHEP* **03** (2020) 101 [arXiv:1910.13432] [INSPIRE].

[148] T. Blum et al., *Hadronic Light-by-Light Scattering Contribution to the Muon Anomalous Magnetic Moment from Lattice QCD*, *Phys. Rev. Lett.* **124** (2020) 132002 [arXiv:1911.08123] [INSPIRE].

[149] G. Colangelo, M. Hoferichter, A. Nyffeler, M. Passera and P. Stoffer, *Remarks on higher-order hadronic corrections to the muon g−2*, *Phys. Lett. B* **735** (2014) 90 [arXiv:1403.7512] [INSPIRE].

[150] S. Borsányi et al., *Leading hadronic contribution to the muon magnetic moment from lattice QCD*, *Nature* **593** (2021) 51 [arXiv:2002.12347] [INSPIRE].

[151] Fermilab Lattice, LATTICE-HPQCD, MILC collaborations, *Strong-Isospin-Breaking Correction to the Muon Anomalous Magnetic Moment from Lattice QCD at the Physical Point*, *Phys. Rev. Lett.* **120** (2018) 152001 [arXiv:1710.11212] [INSPIRE].

[152] Budapest-Marseille-Wuppertal collaboration, *Hadronic vacuum polarization contribution to the anomalous magnetic moments of leptons from first principles*, *Phys. Rev. Lett.* **121** (2018) 022002 [arXiv:1711.04980] [INSPIRE].

[153] RBC, UKQCD collaborations, *Calculation of the hadronic vacuum polarization contribution to the muon anomalous magnetic moment*, *Phys. Rev. Lett.* **121** (2018) 022003 [arXiv:1801.07224] [INSPIRE].

[154] D. Giusti, V. Lubicz, G. Martinelli, F. Sanfilippo and S. Simula, *Electromagnetic and strong isospin-breaking corrections to the muon $g-2$ from Lattice QCD+QED*, *Phys. Rev. D* **99** (2019) 114502 [arXiv:1901.10462] [INSPIRE].

[155] PACS collaboration, *Hadronic vacuum polarization contribution to the muon $g-2$ with 2+1 flavor lattice QCD on a larger than (10 fm)^4 lattice at the physical point*, *Phys. Rev. D* **100** (2019) 034517 [arXiv:1902.00885] [INSPIRE].

[156] Fermilab Lattice, LATTICE-HPQCD, MILC collaborations, *Hadronic-vacuum-polarization contribution to the muon's anomalous magnetic moment from four-flavor lattice QCD*, *Phys. Rev. D* **101** (2020) 034512 [arXiv:1902.04223] [INSPIRE].

[157] A. Gérardin et al., *The leading hadronic contribution to $(g-2)_\mu$ from lattice QCD with $N_\mathrm{f} = 2 + 1$ flavours of O(a) improved Wilson quarks*, *Phys. Rev. D* **100** (2019) 014510 [arXiv:1904.03120] [INSPIRE].

JHEP11(2022)139

[158] C. Aubin, T. Blum, C. Tu, M. Golterman, C. Jung and S. Peris, *Light quark vacuum polarization at the physical point and contribution to the muon $g-2$*, *Phys. Rev. D* **101** (2020) 014503 [arXiv:1905.09307] [INSPIRE].

[159] D. Giusti and S. Simula, *Lepton anomalous magnetic moments in Lattice QCD+QED*, *PoS* **LATTICE2019** (2019) 104 [arXiv:1910.03874] [INSPIRE].

[160] A. Cerri et al., *Report from Working Group 4*: Opportunities in Flavour Physics at the HL-LHC and HE-LHC, *CERN Yellow Rep. Monogr.* **7** (2019) 867 [arXiv:1812.07638] [INSPIRE].

[161] FCC collaboration, *FCC Physics Opportunities*: Future Circular Collider Conceptual Design Report Volume 1, *Eur. Phys. J. C* **79** (2019) 474 [INSPIRE].

[162] C.-Y. Chen, S. Dawson and M. Sher, *Heavy Higgs Searches and Constraints on Two Higgs Doublet Models*, *Phys. Rev. D* **88** (2013) 015018 [*Erratum ibid.* **88** (2013) 039901] [arXiv:1305.1624] [INSPIRE].

[163] C.-Y. Chen and S. Dawson, *Exploring Two Higgs Doublet Models Through Higgs Production*, *Phys. Rev. D* **87** (2013) 055016 [arXiv:1301.0309] [INSPIRE].

[164] P. Bechtle, O. Brein, S. Heinemeyer, G. Weiglein and K.E. Williams, *HiggsBounds: Confronting Arbitrary Higgs Sectors with Exclusion Bounds from LEP and the Tevatron*, *Comput. Phys. Commun.* **181** (2010) 138 [arXiv:0811.4169] [INSPIRE].

[165] P. Bechtle, O. Brein, S. Heinemeyer, G. Weiglein and K.E. Williams, *HiggsBounds 2.0.0: Confronting Neutral and Charged Higgs Sector Predictions with Exclusion Bounds from LEP and the Tevatron*, *Comput. Phys. Commun.* **182** (2011) 2605 [arXiv:1102.1898] [INSPIRE].

[166] P. Bechtle et al., *Recent Developments in HiggsBounds and a Preview of HiggsSignals*, *PoS* **CHARGED2012** (2012) 024 [arXiv:1301.2345] [INSPIRE].

[167] P. Bechtle et al., HiggsBounds – 4*: Improved Tests of Extended Higgs Sectors against Exclusion Bounds from LEP, the Tevatron and the LHC*, *Eur. Phys. J. C* **74** (2014) 2693 [arXiv:1311.0055] [INSPIRE].

[168] P. Bechtle, S. Heinemeyer, O. Stal, T. Stefaniak and G. Weiglein, *Applying Exclusion Likelihoods from LHC Searches to Extended Higgs Sectors*, *Eur. Phys. J. C* **75** (2015) 421 [arXiv:1507.06706] [INSPIRE].

[169] P. Bechtle et al., *HiggsBounds-5: Testing Higgs Sectors in the LHC 13 TeV Era*, *Eur. Phys. J. C* **80** (2020) 1211 [arXiv:2006.06007] [INSPIRE].

[170] H. Bahl, V.M. Lozano, T. Stefaniak and J. Wittbrodt, *Testing exotic scalars with HiggsBounds*, *Eur. Phys. J. C* **82** (2022) 584 [arXiv:2109.10366] [INSPIRE].

[171] M. Krause, M. Mühlleitner and M. Spira, *2HDECAY —A program for the calculation of electroweak one-loop corrections to Higgs decays in the Two-Higgs-Doublet Model including state-of-the-art QCD corrections*, *Comput. Phys. Commun.* **246** (2020) 106852 [arXiv:1810.00768] [INSPIRE].

[172] A. Djouadi, J. Kalinowski and M. Spira, *HDECAY: A Program for Higgs boson decays in the standard model and its supersymmetric extension*, *Comput. Phys. Commun.* **108** (1998) 56 [hep-ph/9704448] [INSPIRE].

[173] A. Djouadi, J. Kalinowski, M. Muehlleitner and M. Spira, *HDECAY: Twenty$_{++}$ years after*, *Comput. Phys. Commun.* **238** (2019) 214 [arXiv:1801.09506] [INSPIRE].

JHEP11(2022)139

[174] M. Krause, M. Muhlleitner, R. Santos and H. Ziesche, *Higgs-to-Higgs boson decays in a 2HDM at next-to-leading order*, *Phys. Rev. D* **95** (2017) 075019 [arXiv:1609.04185] [INSPIRE].

[175] A. Denner, S. Dittmaier and J.-N. Lang, *Renormalization of mixing angles*, *JHEP* **11** (2018) 104 [arXiv:1808.03466] [INSPIRE].

[176] T. Hahn and M. Pérez-Victoria, *Automatized one loop calculations in four-dimensions and D-dimensions*, *Comput. Phys. Commun.* **118** (1999) 153 [hep-ph/9807565] [INSPIRE].

[177] J. Alwall et al., *The automated computation of tree-level and next-to-leading order differential cross sections, and their matching to parton shower simulations*, *JHEP* **07** (2014) 079 [arXiv:1405.0301] [INSPIRE].

[178] ALEPH, DELPHI, L3, OPAL, LEP collaborations, *Search for Charged Higgs bosons: Combined Results Using LEP Data*, *Eur. Phys. J. C* **73** (2013) 2463 [arXiv:1301.6065] [INSPIRE].

[179] CMS collaboration, *Search for physics beyond the standard model in multilepton final states in proton-proton collisions at* $\sqrt{s} = 13$ *TeV*, *JHEP* **03** (2020) 051 [arXiv:1911.04968] [INSPIRE].

[180] CMS collaboration, *Search for charged Higgs bosons in the* $H^{\pm} \to \tau^{\pm}\nu_{\tau}$ *decay channel in proton-proton collisions at* $\sqrt{s} = 13$ *TeV*, *JHEP* **07** (2019) 142 [arXiv:1903.04560] [INSPIRE].

[181] ATLAS collaboration, *Search for charged Higgs bosons decaying into a top-quark and a bottom-quark at* $\sqrt{s} = 13$ *TeV with the ATLAS detector*, ATLAS-CONF-2020-039, CERN, Geneva (2020).

[182] ALEPH, DELPHI, L3, OPAL, LEP Working Group for Higgs Boson Searches collaborations, *Search for neutral MSSM Higgs bosons at LEP*, *Eur. Phys. J. C* **47** (2006) 547 [hep-ex/0602042] [INSPIRE].

[183] ATLAS collaboration, *Search for resonances in the 65 to 110 GeV diphoton invariant mass range using 80* fb^{-1} *of pp collisions collected at* $\sqrt{s} = 13$ *TeV with the ATLAS detector*, ATLAS-CONF-2018-025, CERN, Geneva (2018).

[184] ATLAS collaboration, *Search for Scalar Diphoton Resonances in the Mass Range* $65 - 600$ *GeV with the ATLAS Detector in pp Collision Data at* $\sqrt{s} = 8$ *TeV*, *Phys. Rev. Lett.* **113** (2014) 171801 [arXiv:1407.6583] [INSPIRE].

[185] ATLAS collaboration, *Search for heavy Higgs bosons decaying into two tau leptons with the ATLAS detector using pp collisions at* $\sqrt{s} = 13$ *TeV*, *Phys. Rev. Lett.* **125** (2020) 051801 [arXiv:2002.12223] [INSPIRE].

[186] LHC Higgs Cross Section Working Group collaboration, *Handbook of LHC Higgs Cross Sections: 4. Deciphering the Nature of the Higgs Sector*, arXiv:1610.07922 [INSPIRE].

[187] P. Basler, S. Dawson, C. Englert and M. Mühlleitner, *Showcasing HH production: Benchmarks for the LHC and HL-LHC*, *Phys. Rev. D* **99** (2019) 055048 [arXiv:1812.03542] [INSPIRE].

[188] G.C. Dorsch, S.J. Huber, K. Mimasu and J.M. No, *Echoes of the Electroweak Phase Transition: Discovering a second Higgs doublet through* $A_0 \to ZH_0$, *Phys. Rev. Lett.* **113** (2014) 211802 [arXiv:1405.5537] [INSPIRE].

JHEP11(2022)139

[189] G.C. Dorsch, S.J. Huber, K. Mimasu and J.M. No, *Hierarchical versus degenerate 2HDM: The LHC run 1 legacy at the onset of run 2*, *Phys. Rev. D* **93** (2016) 115033 [arXiv:1601.04545] [INSPIRE].

[190] D. Gonçalves, A. Kaladharan and Y. Wu, *Electroweak phase transition in the 2HDM: Collider and gravitational wave complementarity*, *Phys. Rev. D* **105** (2022) 095041 [arXiv:2108.05356] [INSPIRE].

[191] W. Su, A.G. Williams and M. Zhang, *Strong first order electroweak phase transition in 2HDM confronting future Z & Higgs factories*, *JHEP* **04** (2021) 219 [arXiv:2011.04540] [INSPIRE].

[192] G.C. Dorsch, S.J. Huber, T. Konstandin and J.M. No, *A Second Higgs Doublet in the Early Universe: Baryogenesis and Gravitational Waves*, *JCAP* **05** (2017) 052 [arXiv:1611.05874] [INSPIRE].

[193] L. Wang, *Inflation, electroweak phase transition, and Higgs searches at the LHC in the two-Higgs-doublet model*, *JHEP* **07** (2022) 055 [arXiv:2105.02143] [INSPIRE].

[194] G.C. Dorsch, S.J. Huber, K. Mimasu and J.M. No, *The Higgs Vacuum Uplifted: Revisiting the Electroweak Phase Transition with a Second Higgs Doublet*, *JHEP* **12** (2017) 086 [arXiv:1705.09186] [INSPIRE].

[195] P. Basler, M. Mühlleitner and J. Müller, *Electroweak Baryogenesis in the CP-Violating Two-Higgs Doublet Model*, arXiv:2108.03580 [INSPIRE].

[196] P. Basler and M. Mühlleitner, *BSMPT (Beyond the Standard Model Phase Transitions): A tool for the electroweak phase transition in extended Higgs sectors*, *Comput. Phys. Commun.* **237** (2019) 62 [arXiv:1803.02846] [INSPIRE].

[197] P. Basler, M. Mühlleitner and J. Müller, *BSMPT v2 a tool for the electroweak phase transition and the baryon asymmetry of the universe in extended Higgs Sectors*, *Comput. Phys. Commun.* **269** (2021) 108124 [arXiv:2007.01725] [INSPIRE].

[198] P.S. Bhupal Dev and A. Pilaftsis, *Maximally Symmetric Two Higgs Doublet Model with Natural Standard Model Alignment*, *JHEP* **12** (2014) 024 [*Erratum ibid.* **11** (2015) 147] [arXiv:1408.3405] [INSPIRE].

JHEP11(2022)139